

AperTO - Archivio Istituzionale Open Access dell'Università di Torino

Application of Ti-in-zircon and Zr-in-rutile thermometers to constrain high-temperature metamorphism in eclogites from the Dabie orogen, central China

This is the author's manuscript

Original Citation:

Availability:

This version is available <http://hdl.handle.net/2318/142443> since 2016-06-01T15:44:21Z

Published version:

DOI:10.1016/j.gr.2013.10.011

Terms of use:

Open Access

Anyone can freely access the full text of works made available as "Open Access". Works made available under a Creative Commons license can be used according to the terms and conditions of said license. Use of all other works requires consent of the right holder (author or publisher) if not exempted from copyright protection by the applicable law.

(Article begins on next page)



UNIVERSITÀ DEGLI STUDI DI TORINO

This Accepted Author Manuscript (AAM) is copyrighted and published by Elsevier. It is posted here by agreement between Elsevier and the University of Turin. Changes resulting from the publishing process - such as editing, corrections, structural formatting, and other quality control mechanisms - may not be reflected in this version of the text. The definitive version of the text was subsequently published in [Liu Y.C., Deng L.P., Gu X.F, Groppo C. & Rolfo F. (2015): *Application of Ti-in-zircon and Zr-in-rutile thermometers to constrain high-temperature metamorphism in eclogites from the Dabie orogen, central China. Gondwana Research, 27, 410-423, <http://dx.doi.org/10.1016/j.gr.2013.10.011>].*

You may download, copy and otherwise use the AAM for non-commercial purposes provided that your license is limited by the following restrictions:

- (1) You may use this AAM for non-commercial purposes only under the terms of the CC-BY-NC-ND license.
- (2) The integrity of the work and identification of the author, copyright owner, and publisher must be preserved in any copy.
- (3) You must attribute this AAM in the following format: Creative Commons BY-NC-ND license (<http://creativecommons.org/licenses/by-nc-nd/4.0/deed.en>), [+ *Digital Object Identifier link to the published journal article on Elsevier's ScienceDirect® platform*]

Abstract

Granulitized eclogites from the Dabie orogen, central China represent deeply subducted mafic lower continental crust of the South China Block and record a complex polymetamorphic evolution during Triassic continental deep subduction and subsequent exhumation. These eclogites were strongly affected by multiple decompression and re-crystallization processes during multistage exhumation, thus making the determination of peak metamorphic conditions particularly challenging. However, the recently calibrated Ti-in-zircon and Zr-in-rutile thermometers provide new tools to estimate the peak and post-peak temperatures. The obtained results suggest that the eclogites experienced a protracted high- T (> 900 °C) metamorphic evolution from high- T /ultrahigh-pressure (UHP) eclogite-facies to UHT/HP granulite-facies conditions, characterized by near-isothermal decompression during the initial stages of exhumation.

Most of the analyzed zircons contain less than 20 ppm Ti and only 5–10% of them contain up to 60–100 ppm Ti, the latter corresponding to metamorphic temperatures of > 900 °C. The occurrence of decompression textures preserved in robust minerals (e.g., low-Na omphacite inclusions coexisting with quartz, rutile and ilmenite in zircon; clinopyroxene + plagioclase + quartz intergrowths after omphacite in garnet) suggests that, even in robust minerals such as zircon, mineral inclusions may have experienced some degrees of decompression breakdown or retrogression. Therefore, Ti concentrations in zircons and Zr concentrations in rutile grains within garnet and zircon, respectively, may have been strongly modified by re-crystallization or re-equilibration. As a result, only few (5–10 %) zircons record their actual crystallization temperatures. In comparison, the rutile inclusions in zircon generally define higher temperatures, likely corresponding to their formation and preservation in a Zr-saturated environment. We therefore suggest that rutile inclusions in zircon are the most suitable candidates for high-grade T estimates, especially in strongly retrogressed eclogites.

This study also provides thermometric evidence that supports the previously

1 51 proposed Neoproterozoic mantle plume that led to the breakup of the supercontinent
2 52 Rodinia, especially along the northern periphery of the South China Block.
3
4 53
5
6 54 *Keywords:* Eclogite; high-temperature metamorphism; Ti-in-zircon and Zr-in-rutile
7
8 55 thermometers; continental deep subduction; multistage exhumation.
9
10 56
11
12
13
14
15
16
17
18
19
20
21
22
23
24
25
26
27
28
29
30
31
32
33
34
35
36
37
38
39
40
41
42
43
44
45
46
47
48
49
50
51
52
53
54
55
56
57
58
59
60
61
62
63
64
65

1. Introduction

Peak and post-peak temperature estimates are crucial for better understanding the genesis and evolution of high-pressure (HP) and ultrahigh-pressure (UHP) eclogites and related metamorphic rocks in subduction zones. However, this task is challenging when investigating high-grade rocks, particularly those formed under extreme metamorphic conditions such as ultrahigh-temperature (UHT) metamorphism (Harley, 1998, 2008; Brown, 2007; Kelsey, 2008; Santosh and Kusky, 2010). Temperatures of > 900 °C are, in fact, higher than the closure temperature of most conventional thermometers (Baldwin et al., 2007). An accurate estimate of peak temperature for high-grade rocks is often hampered by the significant re-equilibration or re-crystallization during retrogression and cooling. This has led to the recent development of trace-element thermometers such as those based on titanium concentration in zircon and zirconium concentration in rutile, which may provide a more precise link between the P – T path and geochronological data (e.g., Watson and Harrison, 2005; Watson et al., 2006; Timms et al., 2011). Since their earlier development, the new Ti-in-zircon and Zr-in-rutile thermometers (Zack et al., 2004; Watson et al., 2006; Ferry and Watson, 2007; Baldwin et al., 2007; Tomkins et al., 2007) have been more and more successfully used to estimate the peak and post-peak temperatures of polymetamorphic rocks (e.g., Zack and Luvizotto, 2006; Spear et al., 2006; Baldwin et al., 2007; Miller et al., 2007; Tomkins et al., 2007; Chen and Li, 2008; Liu et al., 2010a; Zhang et al., 2010; Jiao et al., 2011; Meyer et al., 2011; Zheng et al., 2011; Kooijman et al., 2012; Ewing et al., 2013).

Zircon and rutile are common accessory minerals in metamorphic rocks. Therefore, although the possibility of diffusive resetting at high temperature may complicate the interpretation of apparent temperatures and zoning profiles (Watson et al., 2006), Ti-in-zircon and Zr-in-rutile thermometers may allow precise temperature estimates of metamorphism (Zack et al., 2004; Spear et al., 2006; Watson et al., 2006; Baldwin et al., 2007; Ferry and Watson, 2007; Page et al., 2007; Tomkins et al., 2007). Zircon is a robust mineral (Dobrzhinetskaya et al., 2003; Watson et al., 2006) and is

1 86 extensively used for U–Pb geochronology, giving useful information about a wide
2 87 range of tectonic events and related processes (e.g., Rubatto et al., 1999; Hermann et
3 88 al., 2001; Möller et al., 2002; Liu et al., 2011a). Furthermore, the Ti-in-zircon
4 89 thermometer has the potential to create an invaluable link between U-Pb ages and
5 90 temperatures measured *in-situ* in zircon (e.g., Baldwin and Brown, 2008): this is
6 91 particularly true for multiple metamorphic rocks, because internal fine-scaled growth
7 92 structures in zircon may be directly correlated with variations in the physicochemical
8 93 conditions and the duration of each metamorphic event (e.g., Rubatto et al., 1999;
9 94 Corfu et al., 2003; Whitehouse and Platt, 2003). Application of this thermometer to
10 95 two typical UHT granulite localities demonstrated that it is a powerful method to
11 96 determine the peak temperatures of zircons (Baldwin et al., 2007). However, there are
12 97 also studies that show zircon re-crystallized post-peak and did not preserve UHT
13 98 temperatures, whereas rutile in the same samples did (Ewing et al., 2013).

27 99 Zr-in-rutile thermometry, based on the Zr content in rutile coexisting with quartz
28 100 and zircon, is an alternative and complementary method for estimating temperature of
29 101 metamorphism, especially useful for eclogites. Earlier calibrations of the Zr-in-rutile
30 102 thermometer focused on the strong effect of temperature (Zack et al., 2004; Watson et
31 103 al., 2006; Ferry and Watson, 2007), without including a correction for pressure. The
32 104 pressure dependence was incorporated into this thermometer with the calibration of
33 105 Tomkins et al. (2007). This revised thermometer has been demonstrated to be a
34 106 reliable method for the estimate of the peak temperatures in UHT rocks (e.g., Jiao et
35 107 al., 2011; Meyer et al., 2011; Kooijman et al., 2012). Also, Luvizotto and Zack (2009)
36 108 obtained Zr-in-rutile temperatures of up to 850–930 °C for rutile from granulite facies
37 109 metapelites from Val Strona and Val d’Ossola, but with significant resetting of
38 110 Zr-in-rutile temperatures to a spread of lower values.

51 111 As a result, a combined Ti-in-zircon and Zr-in-rutile thermometry is required to
52 112 constrain peak and post-peak metamorphic temperatures for eclogites and related
53 113 high-grade rocks involved in complex processes. A suitable lithology to usefully apply
54 114 these two novel techniques is the granulitized eclogites of the Luotian dome in the
55 115 southwestern part of the North Dabie complex zone (NDZ), central China, which is a

1 116 portion of deeply subducted mafic lower continental crust of the South China Block
2 117 (Liu et al., 2007a). The eclogites underwent UHP and HP eclogite-facies
3 118 metamorphism, followed by HP granulite-facies overprint and later amphibolite-facies
4 119 retrogression, during continental subduction and exhumation (Liu et al., 2011b). The
5 120 peak metamorphic assemblages and compositions of such UHP rocks are commonly
6 121 obliterated or overprinted by subsequent retrograde metamorphism at UHT
7 122 (905–917 °C) conditions (Liu et al., 2011b). These metamorphic temperatures
8 123 approximated or exceeded the closure temperatures of the Fe–Mg exchange
9 124 thermometer between garnet and clinopyroxene (e.g., Raheim and Green, 1974;
10 125 Baldwin et al., 2007). In this context, it is generally difficult, using conventional
11 126 geothermometers, to precisely constrain the actual metamorphic temperatures
12 127 experienced by the eclogites during the various stages of their evolution; nevertheless
13 128 this information is essential for a robust understanding of the genetic and evolutionary
14 129 processes of the UHP rocks in the NDZ.

15 130 Zircon is extremely robust to thermal disturbance and its U–Pb and REE
16 131 systematics can remain preserved despite multiple (U)HT metamorphic episodes and
17 132 re-equilibration, thus providing reliable ages and genetic information (Kooijman et al.,
18 133 2011; and references therein). Although the NDZ eclogites experienced a complex
19 134 metamorphic evolution and multistage retrograde overprinting, zircons from the
20 135 eclogites still preserve multiple metamorphic age-records with REE and mineral
21 136 inclusion constraints (Liu et al., 2011a). Combining the zircon U–Pb ages and the
22 137 estimated temperatures and pressures, the whole P – T – t path of the eclogites during
23 138 subduction and exhumation may be therefore constrained in detail. In this study, we
24 139 applied Ti-in-zircon and Zr-in-rutile thermometers to the NDZ granulitized eclogites.
25 140 The results provide unambiguous evidence of a multistage high- T evolution in the
26 141 NDZ. In addition, the applicability of the zircon and rutile thermometers to
27 142 granulitized eclogites is tested. The implications of our results on the P – T – t evolution
28 143 of the NDZ are discussed, shedding new light on the formation and exhumation of the
29 144 UHP metamorphic belt in the Dabie orogen.

30 145

2. Geological setting

The Dabie orogen is a well known UHP terrain, located in the intermediate segment of the Qinling-Dabie-Sulu orogenic belt formed by the Triassic continental collision between the North China Block and South China Block. It comprises several fault-bounded terranes with varying metamorphic grades and evolutionary histories, and is subdivided into five major lithotectonic units from north to south (Xu et al., 2003; Liu et al. 2007a): (1) the Beihuaiyang zone (BZ); (2) the North Dabie complex zone (NDZ); (3) the Central Dabie UHP metamorphic zone (CDZ); (4) the South Dabie low-*T* eclogite zone (SDZ); and (5) the Susong complex zone (SZ) (Fig. 1). These zones are separated by the Xiaotian-Mozitan fault, Wuhe-Shuihou fault, Hualiangting-Mituo fault and Taihu-Shanlong fault, respectively. Zone (1) is a low-grade composite unit comprising the Foziling (or Xinyang) Group and the Luzhanguan (or Guishan) complex, whereas Zones (2), (3), (4) and (5) belong to the subducted South China Block (Xu et al., 2003, 2005; Liu et al., 2005, 2007a, 2010b, 2011a; Liu and Li, 2008).

A variety of UHP metamorphic rocks, including eclogite, gneiss, quartz jadeitite, schist and impure marble with eclogite nodules, occur in the CDZ and SDZ (e.g., Xu et al., 1992; Okay, 1993; Okay et al., 1993; Rolfo et al., 2004; Li et al., 2004). The occurrence of diamond and coesite in the metamorphic rocks from the CDZ indicates that the UHP metamorphism occurred at 700–850 °C and > 2.8 GPa (e.g., Okay et al., 1989; Wang et al., 1989; Xu et al., 1992; Okay, 1993; Rolfo et al., 2004), whereas the peak *P–T* conditions of the eclogites in the SDZ were estimated at 670 °C and 3.3 GPa (Li et al., 2004). In both the CDZ and SDZ units the UHP eclogite-facies stage was followed by HP eclogite- and amphibolite-facies retrograde metamorphism (e.g., Xu et al., 1992; Rolfo et al., 2004; Li et al., 2004).

The NDZ mainly consists of tonalitic and granitic orthogneisses and post-collisional intrusions with subordinate meta-peridotite (including dunite, harzburgite and lherzolite), garnet pyroxenite, garnet-bearing amphibolite, granulite and eclogite. The oriented mineral exsolutions in garnet and clinopyroxene, and the

1 175 occurrence of micro-diamond imply that the NDZ eclogites underwent UHP
2 176 metamorphism at $P > 3.5$ GPa (Xu et al., 2003, 2005; Liu et al., 2005; Malaspina et al.,
3
4 177 2006). The Triassic zircon U-Pb ages (Liu et al., 2000, 2007a, 2011a; Wang et al.,
5
6 178 2012) and Sm-Nd ages (Liu et al., 2005) of the eclogites from the NDZ suggest that
7
8 179 these rocks formed by the Triassic subduction of the South China Block, similarly to
9
10 180 those from the CDZ and SDZ. The Triassic metamorphic ages (Liu et al., 2000, 2007b;
11
12 181 Xie et al., 2010) and the occurrence of micro-diamond in zircon and garnet (Liu et al.,
13
14 182 2007b) from the NDZ banded gneisses suggest that also the gneisses hosting the
15
16 183 eclogites were involved in the deep subduction of the South China Block, thus
17
18 184 implying that the NDZ experienced UHP metamorphism as a coherent unit. After the
19
20 185 UHP and HP eclogite facies metamorphism, the NDZ eclogites experienced
21
22 186 granulite-facies overprinting and later amphibolite-facies retrogression (e.g., Xu et al.,
23
24 187 2000; Liu et al., 2001, 2005, 2007a). This corroborates the case for a distinct
25
26 188 evolution in the different slices of the Dabie UHP belt. That is, although the three
27
28 189 eclogite-bearing units, *i.e.* the SDZ, CDZ and NDZ, all experienced UHP
29
30 190 metamorphism, they had different exhumation histories, suggesting that they represent
31
32 191 decoupled UHP slices and most probably represent different levels of crustal rocks
33
34 192 (see Liu and Li, 2008 for a review).

35
36
37 193 The Luotian dome in the southwestern segment of the NDZ is a deeply eroded
38
39 194 area with both felsic and mafic granulite lenses (Chen et al., 1998, 2006; Liu et al.,
40
41 195 2007a; Wu et al., 2008). The eclogite occurs as lenses or blocks in garnet-bearing
42
43 196 granitic migmatitic orthogneiss (Liu et al., 2007a). They preserve early
44
45 197 granulite-facies mineral relics and have been overprinted by regionally pervasive HP
46
47 198 granulite-facies metamorphism, followed by penetrative amphibolite-facies
48
49 199 retrogression during exhumation. The eclogite-facies assemblage consists of garnet
50
51 200 and relict omphacite, with rutile, quartz, allanite and fluoro-apatite as common
52
53 201 additional constituents. Although the precise time–temperature cooling history is still
54
55 202 not well-known in detail, the studies by Liu et al. (2007a, 2011b) showed that the
56
57 203 NDZ underwent a complex multistage evolution characterized by a nearly isothermal
58
59 204 decompression during the early stages of exhumation. In particular, five metamorphic
60
61
62
63
64
65

1 205 stages have been recognized for the eclogites in the Luotian dome area (Liu et al.,
2 206 2007a, 2011b): (1) granulite-facies stage, suggested by the occurrence of hypersthene,
3 207 plagioclase and diopside inclusions within garnet and/or by Neoproterozoic
4 208 metamorphic zircon (Liu et al., 2007a); (2) UHP coesite/diamond eclogite-facies stage
5 209 at $P \sim 4.0$ GPa, suggested by the occurrence of diamond (Xu et al., 2003, 2005; Liu et
6 210 al., 2007b) and coesite (Liu et al., 2011b); (3) HP quartz eclogite-facies stage,
7 211 characterized by the coexistence of garnet, jadeite-poor omphacite and rutile with
8 212 quartz instead of coesite; (4) granulite-facies retrogression stage, indicated by the
9 213 presence of hypersthene, plagioclase and diopside symplectite after Na-clinopyroxene;
10 214 (5) amphibolites-facies retrograde stage, documented by the widespread growth of
11 215 amphibole. However, P–T conditions, especially temperatures for different stages
12 216 have not been better constrained because of multiple decompression and
13 217 re-crystallization processes as mentioned above.
14
15
16
17
18
19
20
21
22
23
24
25
26
27
28

29 219 **3. Sample descriptions**

30 220 The investigated samples were collected from Banchuanshan (samples LT9 and
31 221 LT10), Luotian (sample 03LT1-1), Jinjiapu (samples 06LT3-2 and 09LT1) and
32 222 Shiqiaopu (samples 07LT6-1 and 09LT2), respectively (Fig. 1). They can roughly be
33 223 divided into two groups based on zircon typologies: the first eclogite type (Type 1;
34 224 samples 03LT1-1, 06LT3-2, 07LT6-1, 09LT1 and 09LT2) contains almost
35 225 homogeneous Triassic metamorphic zircons with rare or even no Neoproterozoic
36 226 zircon cores (Liu et al., 2011a; Gu, 2012), whereas the second type (Type 2; samples
37 227 LT9 and LT10) contains Neoproterozoic igneous and metamorphic zircon cores with
38 228 rare Triassic metamorphic overgrowth rims (Liu et al., 2007a).

39 229 The detailed ages of the samples LT9, LT10, 03LT1-1, 06LT3-2, 07LT6-1 and
40 230 09LT2 were reported in Liu et al. (2007a, 2011a) and Gu (2012), respectively (see
41 231 also Table 2). Based on previous investigations (Liu et al., 2011a; Gu, 2012), by CL
42 232 images, inclusion assemblages, REE patterns and ages, the
43 233 metamorphic/metamorphosed zircons from samples of the Type 1 eclogites can be
44
45
46
47
48
49
50
51
52
53
54
55
56
57
58
59
60
61
62
63
64
65

1 234 subdivided into two episodes of mantle domains (called inner- and outer-mantles,
2 235 named as M1 and M2) with distinct age-records of 230–220 Ma and 220–210 Ma,
3 236 cluster at 226 ± 2 Ma and 214 ± 2 Ma, respectively. These two zircon domains grew
4 237 in distinct stages of the eclogites metamorphic evolution because they show UHP and
5 238 HP eclogite-facies signatures of Ca-rich garnet + omphacite (Jd = 40–50) + coesite +
6 239 rutile and Mn-rich garnet + omphacite (Jd = 20–30) + quartz + rutile, respectively
7 240 (Liu et al., 2011a; Gu, 2012). Rare thin overgrowth rims of 209–207 Ma and 200–190
8 241 Ma, formed at granulite- and amphibolite-facies stages, respectively, are locally
9 242 observed in zircon.

10 243 Details of the petrography and mineral chemistry of the eclogites were given in
11 244 Liu et al. (2007a, 2011b) and are only summarized here. Samples LT9 and LT10
12 245 consist of garnet, omphacite and rutile and retrograde quartz, diopside, hypersthene,
13 246 hornblende, plagioclase and ilmenite. Sample 03LT1-1 is a strongly retrogressed
14 247 eclogite, mainly consisting of garnet, rutile, hornblende and plagioclase with minor
15 248 quartz, diopside, hypersthene and ilmenite. Rare coesite in zircon and its
16 249 pseudomorphs with radial fractures in garnet were observed (Liu et al., 2011b). The
17 250 other eclogite samples (06LT3-2, 07LT6-1, 09LT1 and 09LT2) are less retrogressed
18 251 and are composed of garnet, omphacite, diopside and rutile, with minor hypersthene,
19 252 hornblende, plagioclase, quartz or its pseudomorphs after coesite and ilmenite. In all
20 253 the samples, omphacite generally occurs as inclusion in garnet or zircon (Figs. 2a, b
21 254 and 3). Two generations of omphacite may be distinguished on the basis of their Na_2O
22 255 contents, the earlier one being Na richer than the later generation (Fig. 4; Table 1).
23 256 The later generation often coexists with quartz in zircon (Fig. 3b, f), suggesting a
24 257 Si-rich precursor omphacite and is locally replaced by clinopyroxene + plagioclase +
25 258 quartz intergrowths in garnet (Fig. 2d). In samples 07LT6-1 and 09LT2 omphacite
26 259 inclusions within garnet and zircon are particularly abundant, and coesite
27 260 pseudomorphs with radial fractures were locally observed within garnet (Figs. 2 and 3;
28 261 Liu et al., 2011b). Furthermore, low-Na omphacite + quartz and rutile + ilmenite
29 262 locally occur as coexisting or intergrowth inclusions in zircon (Figs. 3b, d, f, l and 5).
30 263 This shows that mineral inclusions in zircon and garnet from the eclogites have been

1 264 strongly modified or broken down during multiple decompression and retrogression,
2 265 also hampering the determination of peak P - T conditions by conventional
3 266 thermobarometry. Thus, in order to better constrain the metamorphic temperatures of
4 267 UHP and HP eclogite-facies stages, the Ti-in-zircon thermometry and Zr-in-rutile
5 268 thermometry on inclusions within zircon and garnet have been applied.
6
7
8
9

10 269

11 270 **4. Analytical methods**

12
13 271 Zircons were separated from the samples by crushing and sieving, followed by
14 272 magnetic and heavy liquid separation and hand-picking under a binocular microscope.
15 273 Representative zircon crystals were prepared for the CL investigations and in-situ
16 274 U-Pb dating and trace-element analyses. They, together with a zircon U-Pb standard
17 275 TEM (417 Ma), were mounted in epoxy, which was then polished until all zircon
18 276 grains were approximately cut in half. The internal zoning patterns of the crystals
19 277 were observed by cathodoluminescence (CL) imaging at the Beijing SHRIMP Center
20 278 and the Institute of Mineral Resources, Chinese Academy of Geological Sciences
21 279 (CAGS) in Beijing. The representative CL images for the sample 07LT6-1 are
22 280 presented in Fig. 3, and the remaining CL images were reported in Liu et al. (2007a,
23 281 2011a) and Gu (2012).
24
25
26
27
28
29
30
31
32
33
34
35
36
37

38 282 Mineral inclusions in zircon were identified using Raman spectroscopy at the
39 283 Continental Dynamics Laboratory, CAGS in Beijing and the CAS Key Laboratory of
40 284 Crust-Mantle Materials and Environments, University of Science and Technology of
41 285 China in Hefei, and/or identified using the electron probe micro analyzer (EPMA) at
42 286 the Institute of Mineral Resources, CAGS in Beijing. The analytical conditions of the
43 287 Raman and EMPA were reported by Liu et al. (2009). Representative Raman spectra
44 288 and compositions of mineral inclusions in zircon are reported in Fig. 5 and Table 1.
45
46
47
48
49
50
51

52 289 The rutile analyses were performed on a JEOL JXA-8230 EPMA at the Institute
53 290 of Mineral Resources, CAGS in Beijing. Accelerating voltage was set at 20 kV with
54 291 100 nA beam current and 3–5 μm beam spot, counting times for Zr, Nb, Cr and Fe
55 292 were 300, 400, 150 and 60 s, respectively. Spectroscopic crystals for Zr, Nb, Cr and
56
57
58
59
60
61
62
63
64
65

1 293 Fe were PETH, PETJ, LIFJ and LIFJ, respectively (corresponding detection limits: 20,
2 294 27, 28 and 43 ppm). A ZrO₂ standard was used to calibrate the peak position of Zr,
3
4 295 and a synthetic rutile was used to inspect the zero-concentration of Zr at the beginning,
5
6 296 middle and at the end of each sequence. Analytical errors were about ± 15 ppm at 1σ
7
8 297 according to counting statistics (Chen and Li, 2008). Optical and CL-images
9
10 298 combined with back-scattered electron (BSE) images were used to select target areas
11
12 299 devoid of cracks or inclusions other than rutile in zircon. Also, the BSE images were
13
14 300 guided to determine the analyzed domains on rutile inclusions in garnet on the thin
15
16 301 sections. Generally, larger rutile grains (> 3 μm in diameter, mostly 5–10 μm or more)
17
18 302 were selected for spot analyses. If SiO₂ contents were above 0.3 wt.% the analysis
19
20 303 was discarded as these data were probably influenced by nearby zircon grains (Zack et
21
22 304 al., 2004). In addition, it has been shown (Boniface et al., 2012) that there are the
23
24 305 lower Zr contents in matrix rutile compared to rutile inclusions in garnet, due to
25
26 306 re-equilibration of the matrix grains during the late-stage mylonitization that affected
27
28 307 the eclogites. So, we analyzed rutile inclusions in garnet and zircon from the samples.

31 308 The Ti contents in zircon from samples LT9, LT10, 03LT1-1, 06LT3-2 and
32
33 309 07LT6-1 were measured using laser ablation multi-collector inductively coupled
34
35 310 plasma mass spectrometer (LA-MC-ICPMS) at Institute of Geology and Geophysics,
36
37 311 the Chinese Academy of Sciences in Beijing. The detailed parameters of the
38
39 312 instrument can be found in Jiao et al. (2011), and the analytical procedure was
40
41 313 previously reported by Yuan et al. (2004). A Geolas-193 laser-ablation microprobe
42
43 314 was attached to a Neptune multi-collector ICPMS. Typical ablation times were 30 to
44
45 315 90 s with a 10 Hz repetition rate and laser power of 100 mJ/pulse, resulting in a pit
46
47 316 depth of 30 to 50 μm . The spot diameter for zircon was 32 μm .

48 317

51 318 **5. Results**

52 319 *5.1. Zr contents in rutile and Zr-in-rutile temperature estimates*

53 320 Calculation of Zr-in-rutile temperatures for rutile inclusions within zircon follows
54
55 321 the pressure-dependent thermometer of Tomkins et al. (2007) at assumed 4.0 GPa and
56
57
58
59
60
61
62
63
64
65

1 322 2.0 GPa for the UHP (M_1 domains) and HP (M_2 domains) eclogite-facies
2 323 metamorphism, respectively and at 1.0 GPa for the granulite-facies stage (rim
3 324 domains) (Liu et al., 2011a; Gu, 2012). The estimation of Zr-in-rutile temperatures for
4 325 rutile inclusions within garnet was made at $P = 4.0$ GPa and 2.0 GPa for the UHP and
5 326 HP eclogite-facies conditions, respectively. The Zr contents and calculated
6 327 temperatures are listed in Tables 2 and 3 and depicted in Figs. 6 and 7.

7 328 Rutile inclusions in zircon mainly occur within mantle domains M_1 and M_2 of
8 329 metamorphic/metamorphosed zircons, formed at UHP and HP eclogite-facies
9 330 conditions, respectively, and a few in overgrowth rims formed at granulite-facies
10 331 conditions. Zirconium concentrations in rutile within garnet and zircon are
11 332 characterized by a large spread, varying from less than 900 to more than 4000 ppm,
12 333 and defining a broad range of calculated temperatures from < 700 to approximately
13 334 1100 °C (Figs. 6, 7). More in detail, the rutile inclusions located in inner-mantle
14 335 domains (M_1) of zircon have the high Zr contents (1030–4310 ppm) and record a
15 336 relatively narrow range of temperatures of 880–1080 °C, mostly 936–1072 °C with an
16 337 average value of 982 °C. Rutile grains included in the outer-mantle domains (M_2) of
17 338 zircon contain Zr contents of 800–5800 ppm and define a wide range of temperatures
18 339 (780–1030 °C), a few 901–1028 °C with an average value of 946 °C. A few rutile
19 340 grains occurring in the rims of zircon give lower temperatures of *c.* 850 °C (Fig. 6). In
20 341 contrast, rutile inclusions within garnet have relatively lower Zr contents of 100–800
21 342 ppm, yielding lower temperatures (600–850 °C at $P = 4.0$ GPa and 600–800 °C at $P =$
22 343 2.0 GPa; Fig. 6a and Table 3).

23 344 24 345 *5.2 Ti contents in zircon and Ti-in-zircon temperatures*

25 346 Ti-in-zircon temperatures were calculated following the experimental calibration
26 347 of Watson et al. (2006). The results for Ti contents in zircon and calculated
27 348 temperatures are listed in Tables 3 and 4 and presented in Figs. 8 and 9. Zircon grains
28 349 in the three Type 1 eclogite samples consist of different domains among which inner
29 350 (M_1) and outer (M_2) mantle domains formed at UHP and HP eclogite-facies
30 351 conditions at ~226 Ma and ~214 Ma, respectively. These UHP and HP domains have

1 352 Ti contents of 2.15–97.8 ppm (Table 4), yielding Ti-in-zircon temperatures of
2 353 620–990 °C. Ti contents in the zircon rim domains are low (< 7 ppm) and indicate a *T*
3 354 of 650–700 °C, except for two granulite-facies overgrowth rims which yield a *T* of
4 355 807–828 °C (Fig. 8). Thus, most of the calculated temperatures for different domains
5 356 of metamorphic zircons are < 800 °C and generally lie at 650 ± 50 °C. Exceptions are
6 357 the 934 °C and the 940 °C, 991 °C results from UHP and HP eclogite-facies zircon
7 358 domains, respectively (Fig. 8). The studied zircons with few igneous cores from the
8 359 Type 1 samples are mostly metamorphic in origin as suggested by the low Th/U
9 360 values, mineral inclusions, Hf-isotopes and CL images (Liu et al., 2011a; Gu, 2012)
10 361 and do not record Ti contents corresponding to earlier magmatic crystallization
11 362 events.

12 363 In the two samples of the Type 2 eclogites, several Neoproterozoic magmatic and
13 364 metamorphic zircon cores with thin Triassic overgrowth rims have been observed (Liu
14 365 et al., 2007a). The cores have Ti contents of 4.3–274 ppm (Table 4), yielding
15 366 Ti-in-zircon temperatures of 670–1149 °C according to the experimental calibration
16 367 of Watson et al. (2006) (Fig. 9). Temperatures mostly fall in the range 670–800 °C
17 368 and a few > 900 °C. The metamorphic overgrowth rims in the Type 2 eclogite zircons
18 369 are too thin to be analyzed by the LA-MC-ICPMS.

19 370

20 371 **6. Discussion**

21 372 *6.1. Metamorphic temperatures at peak and post-peak stages*

22 373 The results of this study show that, although all the samples experienced the same
23 374 metamorphic evolution, only 5–10% of the Triassic peak and post-peak metamorphic
24 375 zircons from the Type 1 eclogites contain sufficient Ti concentrations to give high-*T*
25 376 conditions (Fig. 8). Temperatures higher than 900 °C are preserved only in one UHP
26 377 and two HP eclogite-facies zircon domains (M1 and M2, respectively), whereas the
27 378 majority of the analyzed zircons give temperatures of 650 ± 50 °C (Fig. 8), probably
28 379 indicating the amphibolite-facies re-equilibration/re-crystallization temperature of the
29 380 Ti-in-zircon thermometer.

1 381 The significant variability of Zr in rutile (Tables 2 and 3) and the resulting scatter
2 382 in calculated temperatures (especially for rutile inclusions in garnet) (Fig. 6) are
3
4 383 probably due to retrograde re-equilibration and/or to local fluid-mediated
5
6 384 re-crystallization during retrogression owing to the occurrence of fractures in garnet
7
8 385 (see Fig. 2c) (Meyer et al., 2011; Kooijman et al., 2012). As a consequence, results of
9
10 386 the Zr-in-rutile thermometry should be treated with caution when dealing with high-*T*
11
12 387 rocks which have undergone pronounced retrogression. In comparison, Zr-in-rutile
13
14 388 thermometry applied on rutile inclusions within zircon, especially those shielded in
15
16 389 the inner- and outer-mantle domains of Triassic zircons, yields 900 to ~1100 °C.

18 390 The high temperature values of 900–1050 °C estimated by both the Ti-in-zircon
19
20 391 and the Zr-in-rutile thermometers for the UHP metamorphic stage are consistent with
21
22 392 the reported peak UHP temperatures of 900–960 °C (at $P = 4.0$ GPa) calculated using
23
24 393 Grt-Cpx thermometry (Liu et al., 2007a). Only one inclusion of rutile was observed in
25
26 394 the overgrowth rims of zircon and records temperatures of 820–850 °C (Fig. 6),
27
28 395 similar to those estimated by Ti-in-zircon thermometry (granulite-facies overgrowth
29
30 396 rims; Fig. 8).

33 397 The Zr-in-rutile and Ti-in-zircon thermometers combined with conventional
34
35 398 thermometry demonstrate that the eclogites experienced a multistage high-*T* (>
36
37 399 900 °C) metamorphic evolution at UHP and HP eclogite-facies conditions, followed
38
39 400 by granulite-facies overprinting at UHT conditions.

41 401 In addition, as to the two samples of the Type 2 eclogites, their Neoproterozoic
42
43 402 magmatic and metamorphic zircon cores yield Ti-in-zircon temperatures of 670–1149
44
45 403 °C (Fig. 9) with temperatures mostly in the range of 670–800 °C and a few > 900 °C.
46
47 404 The highest temperature values of > 900 °C may be the closest to the real
48
49 405 temperatures (Liu et al., 2010a), thus for the first time documenting a UHT
50
51 406 metamorphism during the Neoproterozoic. In contrast, the lower temperatures might
52
53 407 represent the result of re-equilibration as suggested by Timms et al. (2011).

54 408

58 409 *6.2. Factors affecting Ti-in-zircon and Zr-in-rutile temperature estimates*

60 410 *5.2.1. Ti-in-zircon thermometer*

1 411 Pre-existing zircon in rocks may re-equilibrate in response to changing P - T
2 412 conditions or fluid compositions (Kooijman et al., 2011). Timms et al. (2011) also
3 413 suggested that the highest Ti-in-zircon temperatures recorded in zircon might
4 414 represent only minimum estimates for primary zircon crystallization and that the
5 415 lowest Ti concentrations might record re-equilibration. Our results are in agreement
6 416 with this interpretation. The analyzed zircons from the NDZ eclogites, in fact, show a
7 417 large spread of Ti concentrations thus defining a wide range of temperatures. These
8 418 strongly variable calculated temperatures may result from two main factors: (i) they
9 419 may correspond to different growth stages of zircon, as suggested by the multiple
10 420 age-records (Liu et al., 2011a, b; Gu, 2012), and/or (ii) they may be related to
11 421 significant re-equilibration processes. However, since zircon domains with different
12 422 ages generally define homogeneous Ti-in-zircon temperatures of 650 ± 50 °C with the
13 423 exception of few high- T values > 900 °C (Figs. 8 and 9), we suggest that the highest
14 424 calculated temperatures may represent the T of zircon growth/crystallization, while
15 425 the lower temperatures probably represent the re-equilibration temperature at
16 426 amphibolite-facies conditions, in agreement with those determined by conventional
17 427 thermobarometry (Liu et al., 2007a) and with the lower temperatures derived from
18 428 Zr-in-rutile thermometry (this study).

19 429

20 430 *6.2.2. Zr-in-rutile thermometer*

21 431 It has been documented that the Zr-in-rutile thermometer is very resistant to
22 432 diffusion and re-equilibration even under UHT metamorphic conditions and can
23 433 preserve peak metamorphic temperatures higher than most thermometers (e.g.,
24 434 Kooijman et al., 2012; Ewing et al., 2013; and references therein). Zack et al. (2004)
25 435 argued that rutile included in mineral phases in which diffusivities are high (e.g.
26 436 quartz, kyanite) generally show significant evidence of re-equilibration during cooling,
27 437 whereas rutile inclusions in garnet generally preserve higher Zr contents than matrix
28 438 rutile. However, conflicting evidence exists on this argument, since other studies (e.g.,
29 439 Baldwin et al., 2007) show little correlation between recorded Zr-in-rutile
30 440 temperatures and the rutile being in the matrix or included in garnet. The diffusion

1 441 data also suggest that Zr signatures of rutiles from UHT systems are likely to be lost
2 442 except under conditions of extremely rapid cooling (Cherniak et al., 2007). Thus, Zr
3
4 443 in rutile signatures from high-*T* contexts may be only locally retained, depending on
5
6 444 the nature of surrounding materials and the effectiveness of diffusional transport
7
8 445 through them (e.g., Zack et al., 2004; Watson et al., 2006).

10 446 In this study, the highest concentrations of Zr are systematically recorded in well
11
12 447 shielded rutile inclusions within zircon, although numerous grains located in the same
13
14 448 mantle and rim domains of zircon preserve low Zr concentrations as well (Figs. 6 and
15
16 449 7; Tables 2 and 3). Thus, being shielded in zircon is not a prerequisite for rutile to
17
18 450 preserve high temperatures. In contrast, rutile inclusions in garnet have systematically
19
20 451 lower Zr contents than those included in zircon (Fig. 6). Previous investigations (e.g.,
21
22 452 Jiao et al., 2011; Meyer et al., 2011; Triebold et al., 2011; Kooijman et al., 2012)
23
24 453 clearly indicate that rutile grains with lower Zr concentrations have been likely
25
26 454 affected by re-equilibration and/or re-crystallization processes, even if included in
27
28 455 robust minerals such as garnet; in this case, the corresponding calculated temperatures
29
30 456 are not representative of the metamorphic conditions of entrapment (see also Hermann
31
32 457 and Rubatto, 2003). Although zircon is probably the best rigid host mineral, this study
33
34 458 demonstrates that some rutile inclusions within zircon were transformed to ilmenite,
35
36 459 thus suggesting that retrogression may affect also zircon and its inclusions (Fig. 3). It
37
38 460 may be thus concluded that rutile grains with higher Zr concentrations (and
39
40 461 corresponding calculated temperatures) should be the least affected by late resetting,
41
42 462 most probably revealing rutile formation temperatures (Triebold et al., 2011), whereas
43
44 463 the lower temperatures of 650–750 °C (Fig. 6) probably represent the closure
45
46 464 temperature of the Zr-in-rutile thermometer (Cherniak et al., 2007) and/or
47
48 465 re-equilibration/re-crystallization temperatures at amphibolites-facies conditions (Liu
49
50 466 et al., 2007a).

51
52
53 467

54 468 *6.2.3. Late re-equilibration processes affecting rutile and zircon*

55
56 469 The widespread and homogeneous low-*T* estimates of 650–750 °C obtained from
57
58 470 both the Zr-in-rutile and Ti-in-zircon thermometers imply that both rutile and zircon

1 471 from the studied NDZ eclogites were significantly affected by re-equilibration or
2 472 re-crystallization processes during exhumation or decompression, as reported by Liu
3 473 et al. (2009), Boniface et al. (2012) and Ewing et al. (2013). Moreover, the wide range
4 474 of calculated temperatures obtained from both thermometers is interpreted to be the
5 475 result of trace element exchange between rutile/zircon and the matrix, this process
6 476 likely occurring at the grain-boundary scale or along the fracture and being controlled
7 477 by fluid-mediated transport within very local domains.

8 478 Furthermore, Lucassen et al. (2010) showed that, in fluid-dominated natural
9 479 systems, the diffusion coefficients of Zr and Nb in rutile could be higher than those
10 480 determined experimentally. Luvizotto and Zack (2009) also argued that
11 481 re-equilibration of Zr in rutile occurs by ion exchange with neighboring minerals in a
12 482 fluid-present system, whereas in the absence of fluids, volume diffusion of Zr in rutile
13 483 is limited by grain boundary diffusion. In this regard, the lower Zr contents of rutile
14 484 inclusions in garnet relative to those in zircon could be due to the effect of fluids,
15 485 likely introduced in garnet through radial fractures (see Fig. 2c) (e.g., Meyer et al.,
16 486 2011). In contrast, zircon is better than garnet in preventing fluid infiltration, so that
17 487 rutile inclusions within zircon may preserve high Zr contents.

18 488 In addition, the high- T (> 900 °C) decompression process during the initial stage
19 489 of exhumation from UHP eclogite facies to granulite facies has led to significant
20 490 partial melting of the eclogites in the region (Liu et al., 2011b; Gu, 2012). This partial
21 491 melting on the zircons might have a marked effect, and only few zircons could survive
22 492 and record the peak metamorphic temperatures (Liu et al., 2009).

23 493 In summary, rutile and zircon are robust enough to preserve compositions from
24 494 earlier stages of a complex metamorphic history, and Zr-in-rutile and Ti-in-zircon
25 495 thermometers have the potential to be very useful tools for estimating crystallization
26 496 temperatures and peak metamorphic conditions. Furthermore, rutile included in a rigid
27 497 phase such as zircon is able to retain its original Zr content. Therefore, for
28 498 (ultra)high- T metamorphic rocks, Zr-in-rutile, especially applied on rutile inclusions
29 499 within zircon, may yield more reliable peak metamorphic temperatures than most
30 500 other exchange geothermometers, which tend to partially re-equilibrate during cooling

1 501 (Kooijman et al., 2012).

2 502

3
4 503 *6.3. Implications for peak metamorphic conditions and high- T exhumation*

5
6 504 Figure 10 shows the P - T - t path of the NDZ eclogites as constrained by
7
8 505 Ti-in-zircon and Zr-in-rutile thermometry (this study), conventional thermometry and
9
10 506 SHRIMP U-Pb ages (Liu et al., 2011a; Gu, 2012). A variety of models for exhumation
11
12 507 of UHP metamorphic rocks from mantle depths have been proposed (e.g., Ernst, 1971,
13
14 508 2001; Chemenda et al., 1995; Maruyama et al., 1996; Hacker et al., 2000; Liu et al.,
15
16 509 2007b). The present and the already published data support a scenario in which the
17
18 510 deeply subducted continental crust of the South China Block did not remain a single
19
20 511 coherent unit, but formed several slices by multiple decoupling during subduction to
21
22 512 mantle depths and subsequent exhumation; this decoupling may have been triggered
23
24 513 by the difference in mechanic strength of rocks occurring at different levels of the
25
26 514 continental crust (Liu et al., 2007b, 2011a; Liu and Li, 2008). Considering the
27
28 515 weighted mean ages of UHP metamorphism (226 Ma) and HP eclogite-facies
29
30 516 retrogression (214 Ma), the exhumation from mantle depths (ca. 4.0 GPa) to crustal
31
32 517 depths of ca. 2.0 GPa must have been completed within about 12 Ma (Fig. 10). This
33
34 518 implies that about 60 km of exhumation should have occurred within about 12 Ma,
35
36 519 leading to an average exhumation rate of 0.5 cm/y. A comparatively lower exhumation
37
38 520 rate of ~ 0.4 cm/y characterized the following evolution from HP eclogite-facies (214
39
40 521 Ma) to granulite-facies (207 Ma) conditions, corresponding to nearly isothermal
41
42 522 exhumation at very high T ($> 900^{\circ}\text{C}$) from pressures of 2.0 to 1.0 GPa. Therefore, the
43
44 523 rapid exhumation rate of the initial stage of exhumation was followed by a
45
46 524 comparatively slower exhumation at UHT conditions, which led to significant partial
47
48 525 melting (Liu et al., 2011b; Gu, 2012). The protracted high- T evolution experienced by
49
50 526 the NDZ eclogites may explain why UHP relicts are rarely preserved in the eclogites
51
52 527 and in the associated rocks from the NDZ. In fact, although a relatively rapid
53
54 528 exhumation is considered to be one of the factors favoring the preservation of UHP
55
56 529 mineral assemblages (e.g., Mosenfelder et al., 2005; Liu et al., 2011b), a long
57
58 530 residence time at high temperatures may have played an opposite role (Katayama and
59
60
61
62
63
64
65

1 531 Maruyama, 2009).

2 532 UHT conditions may be reached in many different tectonic environments
3
4 533 (Santosh and Kusky, 2010) whereas the heat source to attain UHT conditions in the
5
6 534 lower crust has been ascribed to asthenospheric mantle upwelling in response to
7
8 535 delamination or thinning of the continental lithosphere (e.g., Harley, 2008). However,
9
10 536 based on the present study, the high temperatures of > 900 °C estimated by
11
12 537 Ti-in-zircon thermometer for the Neoproterozoic magmatism and granulite facies
13
14 538 metamorphism in the NDZ could have been caused by a mantle plume, or an
15
16 539 asthenospheric upwelling in response to large-scale continental rifting, resulting from
17
18 540 the breakup of Rodinia at the Neoproterozoic in the South China Block (Ames et al.,
19
20 541 1996; Rowley et al., 1997; Li et al., 2003; Liu et al., 2007a, 2010b). Recent works
21
22 542 (e.g., Whittington et al., 2009; Santosh and Kusky, 2010) suggest that the lower crust
23
24 543 has a low thermal diffusivity and is therefore able to retain heat for long time and that
25
26 544 the underlying mantle has a higher mean temperature. Thus, in the case of extensional
27
28 545 settings such as the continental rift zones, the heat and volatiles supplied by rising
29
30 546 plumes might contribute to the generation of UHT metamorphism in the lower crust
31
32 547 (Santosh and Kusky, 2010). In this context, the underplating and injection of the
33
34 548 high-temperature melts may have triggered extensive crustal anatexis, producing large
35
36 549 volumes of granitoids and associated basaltic rocks (precursors for most of UHP
37
38 550 meta-igneous rocks in the Dabie-Sulu orogenic belt) along the periphery of the South
39
40 551 China Block, and local UHT metamorphism in the Neoproterozoic. Furthermore,
41
42 552 petrological and geochronological studies have demonstrated that the eclogites
43
44 553 described in this study derived from Neoproterozoic mafic granulites (Liu et al.
45
46 554 2007a). In other words, the protolith of the eclogite was a mafic granulite that
47
48 555 originated from underplating of mantle-derived magma onto the base of lower
49
50 556 continental crust during the mid-Neoproterozoic (ca. 800 Ma) and was then subducted
51
52 557 during the Triassic, experiencing UHP eclogite facies metamorphism at mantle depths.
53
54 558 Therefore, this study provides additional thermometric evidence for the proposed
55
56 559 Neoproterozoic mantle plume that led to the breakup of the supercontinent Rodinia,
57
58 560 especially along the periphery of the South China Block.
59
60
61
62
63
64
65

561

562 **7. Conclusions**

563 The temperatures estimated using zircons and rutile inclusions within zircon from
564 the NDZ granulitized eclogites reveal a protracted high- T (> 900 °C) metamorphic
565 history with at least three metamorphic stages, that occurred at significantly different
566 pressures and ages, during Triassic continental subduction and subsequent exhumation.
567 The investigated rutiles occur as inclusions in both garnet and zircon, and contain
568 different Zr concentrations corresponding to different ranges of calculated
569 temperatures. Rutile inclusions within zircons have the highest Zr concentrations,
570 corresponding to $T > 900$ °C. However, only 5–10% of the analyzed zircons record
571 these high- T conditions. Considering the significantly variable concentrations of Zr in
572 rutile inclusions within garnet, the resulting broadly scattered calculated temperatures
573 are probably related to retrograde re-equilibration and/or to local re-crystallization
574 during retrogression. On the contrary, rutile inclusions within zircon are able to
575 preserve primary compositions even at high- T conditions (> 900 °C) yielding reliable
576 temperatures for rutile crystallization and peak metamorphic conditions.

577 The present temperature estimates, combined with petrological observations and
578 geochronological results, further suggest that the eclogite in the NDZ experienced a
579 clockwise trajectory with a near-isothermal decompression path under high- T
580 conditions, multistage exhumation and rapid uplift during the early stages of
581 exhumation. This protracted high- T persistence with slow cooling may explain the
582 rare preservation of UHP assemblages and compositions in the NDZ.

583 Finally, this study provides robust thermometric evidence in support of the
584 previously proposed Neoproterozoic mantle plume that led to the breakup of the
585 supercontinent Rodinia, especially along the northern periphery of the South China
586 Block.

587

588 **Acknowledgments**

589 This study was supported by funds from the National Basic Research Program of

1 590 China (2009CB825002), the National Natural Science Foundation of China
2
3 591 (41273036, 40921002 and 40973043) and the PhD Foundation of the Ministry of
4
5 592 Education of China (200803580001). Special thanks are due to J.-H. Yang and Y.-H.
6
7 593 Yang for trace-element analysis on zircon, and Z.-Y. Chen for electron microprobe
8
9 594 analysis.
10
11 595

1
2
3
4
5
6
7
8
9
10
11
12
13
14
15
16
17
18
19
20
21
22
23
24
25
26
27
28
29
30
31
32
33
34
35
36
37
38
39
40
41
42
43
44
45
46
47
48
49
50
51
52
53
54
55
56
57
58
59
60
61
62
63
64
65

596 **References**

- 597 Ames, L., Zhou, G., Xiong, B., 1996. Geochronology and isotopic character of
598 ultrahigh-pressure metamorphism with implications for collision of the
599 Sino-Korean and Yangtze cratons, central China. *Tectonics* 15, 472–489.
- 600 Baldwin, J.A., Brown, M., Schmitz, M.D., 2007. First application of
601 titanium-in-zircon thermometry to ultrahigh-temperature metamorphism. *Geology*
602 35, 295–298.
- 603 Baldwin, J.A., Brown, M., 2008. Age and duration of ultrahigh-temperature
604 metamorphism in the Anápolis–Itaucu Complex, Southern Brasília Belt, central
605 Brazil — constraints from U–Pb geochronology, mineral rare earth element
606 chemistry and trace-element thermometry. *Journal of Metamorphic Geology* 26,
607 213–233.
- 608 Blundy, J.D., Holland, T.J.B., 1990. Calcic amphibole equilibria and a new
609 amphibole-plagioclase geothermometer. *Contributions to Mineralogy and*
610 *Petrology* 104, 208–224.
- 611 Boniface, N., Schenk, V., Appel, P., 2012. Paleoproterozoic eclogites of MORB-type
612 chemistry and three Proterozoic orogenic cycles in the Ubendian Belt (Tanzania):
613 Evidence from monazite and zircon geochronology, and geochemistry.
614 *Precambrian Research* 192–195, 16–33.
- 615 Brown, M., 2007. Metamorphism, plate tectonics and the supercontinent cycle. *Earth*
616 *Science Frontiers* 14, 1–18.
- 617 Bruno, M., Compagnoni, R., Rubbo, M., 2001. The ultra-high pressure coronitic and
618 pseudomorphous reactions in a metagranodiorite from the Brossasco-Isasca Unit,
619 Dora-Maira Massif, western Italian Alps: a petrographic study equilibrium
620 thermodynamic modeling. *Journal of Metamorphic Geology* 19, 33–43.
- 621 Chemenda, A.I., Mattauer, M., Malavieille, J., Bokun, A.N., 1995. A mechanism for
622 syn-collisional rock exhumation and associated normal faulting: results from
623 physical modeling. *Earth and Planetary Science Letters* 132, 225–232.
- 624 Chen, N.S., Sun, M., You, Z.D., Malpas, J., 1998. Well-preserved garnet growth
625 zoning in granulite from the Dabie Mountains, central China. *Journal of*

- 1 626 Metamorphic Geology 16, 213–222.
- 2 627 Chen, Y., Ye, K., Liu, J.B., Sun, M., 2006. Multistage metamorphism of the
- 3
- 4 628 Huangtuling granulite, Northern Dabie Orogen, eastern China: implications for
- 5
- 6 629 the tectonometamorphic evolution of subducted lower continental crust. *Journal*
- 7
- 8 630 *of Metamorphic Geology* 24, 633–654.
- 9
- 10 631 Chen, Z.Y., Li, Q.L., 2008. Zr-in-rutile thermometry in eclogite at Jinheqiao in the
- 11
- 12 632 Dabie orogen and its geochemical implications. *Chinese Science Bulletin* 53,
- 13
- 14 633 768–776.
- 15
- 16 634 Cherniak, D.J., Manchester, J., Watson, E.B., 2007. Zr and Hf diffusion in rutile. *Earth*
- 17
- 18 635 *and Planetary Science Letters* 262, 267–279.
- 19
- 20
- 21 636 Corfu, F., Hanchar, J.M., Hoskin, P.W.O., Kinny, P., 2003. Atlas of zircon textures.
- 22
- 23
- 24 637 *Reviews in Mineralogy and Geochemistry* 53, 469–500.
- 25
- 26
- 27 638 Dobrzhinetskaya, L.F., Green, H.W., Bozhilov, K.N., Mitchell, T.E., Dickerson, R.M.,
- 28
- 29 639 2003. Crystallization environment of Kazakhstan microdiamond: evidence from
- 30
- 31 640 nanometric inclusions and mineral associations. *Journal of Metamorphic Geology*
- 32
- 33 641 21, 425–437.
- 34
- 35
- 36
- 37 642 Ellis, D.J., Green, D.H., 1979. An experimental study of the effect of Ca upon
- 38
- 39 643 garnet-clinopyroxene Fe-Mg exchange equilibration. *Contributions to Mineralogy*
- 40
- 41 644 *and Petrology* 71, 13–22.
- 42
- 43
- 44 645 Ernst, W.G., 1971. Metamorphic zonations on presumably subducted lithospheric
- 45
- 46 646 plates from Japan, California and the Alps. *Contributions to Mineralogy and*
- 47
- 48 647 *Petrology* 34, 43–59.
- 49
- 50 648 Ernst, W.G., 2001. Subduction, ultrahigh-pressure metamorphism, and regurgitation of
- 51
- 52 649 buoyant crustal slices—implications for arcs and continental growth. *Physics of*
- 53
- 54 650 *the Earth and Planetary Interiors* 127, 253–275.
- 55
- 56 651 Ewing, T.A., Hermann, J., Rubatto, D., 2013. The robustness of the Zr-in-rutile and
- 57
- 58 652 Ti-in-zircon thermometers during high-temperature metamorphism
- 59
- 60 653 (Ivrea-Verbano Zone, northern Italy). *Contributions to Mineralogy and Petrology*

- 654 165, 757–779.
- 655 Ferry, J.M., Watson, E.B., 2007. New thermodynamic models and revised calibrations
656 for the Ti-in-zircon and Zr-in-rutile thermometers. *Contributions to Mineralogy
657 and Petrology* 154, 429–437.
- 658 Fitzsimons, I.C.W., Harley, S.L., 1994. The influence of retrograde cation exchange
659 on granulite P–T estimates and a convergence technique for the recovery of peak
660 metamorphic conditions. *Journal of Petrology* 35, 543–576.
- 661 Frost, B.R., Chacko, T., 1989. The granulite uncertainty principle: limitations on the
662 thermometry in granulites. *Journal of Geology* 97, 435–450.
- 663 Fu, B., Page, F.Z., Cavosie, A.J., Clechenko, C.C., Fournelle, J., Kita, N.T., Lackey,
664 J.S., Wilde, S.A., Valley, J.W., 2008. Ti-in-zircon thermometry: applications and
665 limitations. *Contributions to Mineralogy and Petrology* 156, 197–215.
- 666 Gebauer, D., Schertl, H.P., Brix, M., Schreyer, W., 1997. 35 Ma old
667 ultrahigh-pressure metamorphism and evidence for very rapid exhumation in the
668 Dora Maira Massif, Western Alps. *Lithos* 41, 5–24.
- 669 Gu, X.F., 2012. Petrologic geochemistry and isotopic geochronology of the Luotian
670 eclogites from the North Dabie complex zone, central China. PhD thesis.
671 University of Science and Technology of China, 165 pp.
- 672 Hacker, B.R., Ratschbacher, L., Webb, L., McWilliams, M.O., Ireland, T., Calvert, A.,
673 Dong, S., Wenk, H.R., Chateigner, D., 2000. Exhumation of ultrahigh-pressure
674 continental crust in east central China: Late Triassic–Early Jurassic tectonic
675 unroofing. *Journal of Geophysical Research* 105, 13339–13364.
- 676 Harley, S.L., 2008. Refining the P–T records of UHT crustal metamorphism. *Journal
677 of Metamorphic Geology* 26, 125–154.
- 678 Harley, S.L., 2008. Refining the P–T records of UHT crustal metamorphism. *Journal
679 of Metamorphic Geology* 26, 125–154.
- 680 Hemingway, B.S., Bohlen, S.R., Hankins, W.B., Westrum, E.J., Kuskov, O.L., 1998.
681 Heat capacity and thermodynamic properties for coesite and jadeite:
682 reexamination of the quartz-coesite equilibrium boundary. *American
683 Mineralogist* 83, 409–418.
- 684 Hermann, J., Rubatto, D., Korsakov, A., Shatsky, V.S., 2001. Multiple zircon growth
685 during fast exhumation of diamondiferous, deeply subducted continental crust

686 (Kokchetav massif, Kazakhstan). *Contributions to Mineralogy and Petrology* 141,
687 66–82.

688 Hermann, J., Rubatto, D., 2003. Relating zircon and monazite domains to garnet
689 growth zones: age and duration of granulite facies metamorphism in the Val
690 Malenco lower crust. *Journal of Metamorphic Geology* 21, 833–852.

691 Jiao, S.J., Guo, J., Mao, Q., Zhao, R., 2011. Application of Zr-in-rutile thermometry: a
692 case study from ultrahigh-temperature granulites of the Khondalite belt, North
693 China Craton. *Contributions to Mineralogy and Petrology* 162, 379–393.

694 Katayama, I., Maruyama, S., 2009. Inclusion study in zircon from ultrahigh-pressure
695 metamorphic rocks in the Kokchetav massif: an excellent tracer of metamorphic
696 history. *Journal of the Geological Society, London* 166, 783–796.

697 Kelsey, D.E., 2008. On ultrahigh-temperature crustal metamorphism. *Gondwana*
698 *Research* 13, 1–29.

699 Kennedy, C.S., Kennedy, G.C., 1976. The equilibrium boundary between graphite and
700 diamond. *Journal of Geophysical Research* 81, 2467–2470.

701 Kooijman, E., Upadhyay, D., Mezger, K., Raith, M.M., Berndt, J., Srikantappa, C.,
702 2011. Response of the U–Pb chronometer and trace elements in zircon to
703 ultrahigh-temperature metamorphism: The Kadavur anorthosite complex,
704 southern India. *Chemical Geology* 290, 177–188.

705 Kooijman, E., Smit, M.A., Mezger, K., Berndt, J., 2012 Trace element systematics in
706 granulite facies rutile: implications for Zr geothermometry and provenance
707 studies. *Journal of Metamorphic Geology* 30, 397–412.

708 Krogh, E.J., 1988. The garnet-clinopyroxene Fe-Mg geothermometer - a
709 reinterpretation of existing Experimental data. *Contributions to Mineralogy and*
710 *Petrology* 99, 44–48.

711 Li, S., Xiao, Y., Liu, D., Ge, N., Zhang, Z., Sun, S.S., Cong, B., Zhang, R.Y., Hart,
712 S.R., Wang, S., 1993. Collision of the North China and Yangtze blocks and
713 formation of coesite-bearing eclogites: Timing and processes. *Chemical Geology*
714 109, 89–111.

715 Li, S., Jagoutz, E., Chen, Y., Li, Q., 2000. Sm–Nd and Rb–Sr isotope chronology of

- 1 716 ultrahigh-pressure metamorphic rocks and their country rocks at Shuanghe in the
2 717 Dabie Mountains, central China. *Geochimica Cosmochimica Acta* 64,
3 718 1077–1093.
- 4
5
6 719 Li, X.P., Zheng, Y.F., Wu, Y.B., Chen, F.K., Gong, B., Li, Y.L., 2004. Low-T eclogite
7 720 in the Dabie terrane of China: petrological and isotopic constrains on fluid
8 721 activity and radiometric dating. *Contributions to Mineralogy and Petrology* 148,
9 722 443–470.
- 10
11 723 Li, Z.X., Li, X.H., Kinny, P.D., Wang, J., Zhang, S., Zhou, H., 2003. Geochronology
12 724 of Neoproterozoic syn-rift magmatism in the Yangtze Craton, South China and
13 725 correlations with other continents: evidence for a mantle superplume that broke
14 726 up Rodinia. *Precambrian Research* 122, 85–109.
- 15
16 727 Liu, S.J., Li, J.H., Santosh, M., 2010a. First application of the revised Ti-in-zircon
17 728 geothermometer to Paleoproterozoic ultrahigh-temperature granulites of
18 729 Tuguiwula, Inner Mongolia, North China Craton. *Contributions to Mineralogy
19 730 and Petrology* 159, 225–235.
- 20
21 731 Liu, Y.-C., Li, S., Xu, S., Li, H., Jiang, L., Chen, G., Wu, W., Su, W., 2000. U-Pb
22 732 zircon ages of the eclogite and tonalitic gneiss from the northern Dabie
23 733 Mountains, China and multi-overgrowths of metamorphic zircons. *Geological
24 734 Journal of China Universities* 6, 17–423 (in Chinese with English abstract).
- 25
26 735 Liu, Y.-C., Xu, S., Li, S., Chen, G., Jiang, L., Zhou, C., Wu, W., 2001. Distribution and
27 736 metamorphic P–T condition of the eclogites from the mafic-ultramafic belt in the
28 737 northern part of the Dabie Mountains. *Acta Geologica Sinica* 75, 385–395 (in
29 738 Chinese with English abstract).
- 30
31 739 Liu, Y.-C., Li, S., Xu, S., Jahn, B.M., Zheng, Y.F., Zhang, Z., Jiang, L., Chen, G., Wu,
32 740 W., 2005. Geochemistry and geochronology of eclogites from the northern Dabie
33 741 Mountains, central China. *Journal of Asian Earth Sciences* 25, 431–443.
- 34
35 742 Liu, Y.-C., Li, S., Gu, X., Xu, S., Chen, G., 2007a. Ultrahigh-pressure eclogite
36 743 transformed from mafic granulite in the Dabie orogen. *Journal of Metamorphic
37 744 Geology* 25, 975–989.
- 38
39 745 Liu, Y.-C., Li, S., Xu, S., 2007b. Zircon SHRIMP U-Pb dating for gneiss in northern

- 1 746 Dabie high T/P metamorphic zone, central China: Implication for decoupling
2 747 within subducted continental crust. *Lithos* 96, 170–185.
- 3
4 748 Liu, Y.-C., Li, S., 2008. Detachment within subducted continental crust and
5 multi-slice successive exhumation of ultrahigh-pressure metamorphic rocks:
6 749 Evidence from the Dabie-Sulu orogenic belt. *Chinese Science Bulletin* 53,
7 750 3105–3119.
- 8
9 751
10
11
12 752 Liu, Y.-C., Wang, A., Rolfo, F., Groppo, C., Gu, X., Song, B., 2009. Geochronological
13 and petrological constraints on Palaeoproterozoic granulite facies metamorphism
14 753 in southeastern margin of the North China Craton. *Journal of Metamorphic
15 754 Geology* 27, 125–138.
- 16
17
18
19 755
20
21 756 Liu, Y.-C., Liu, L., Gu, X., Li, S., Liu, J., Song, B., 2010b. Occurrence of
22 Neoproterozoic low-grade metagranite in the western Beihuaiyang zone, the
23 757 Dabie orogen. *Chinese Science Bulletin* 55, 3490–3498.
- 24
25
26
27 758
28
29 759 Liu, Y.C., Gu, X., Li, S., Hou, Z.H., Song, B., 2011a. Multistage metamorphic events
30 in granulitized eclogites from the North Dabie complex zone, central China:
31 760 evidence from zircon U-Pb age, trace element and mineral inclusion. *Lithos* 122,
32 761 107–121.
- 33
34
35 762
36 763 Liu, Y.-C., Gu, X., Rolfo, F., Chen, Z., 2011b. Ultrahigh-pressure metamorphism and
37 764 multistage exhumation of eclogite from the Luotian dome, North Dabie Complex
38 765 Zone (central China): Evidence from mineral inclusions and decompression
39 766 texture. *Journal of Asian Earth Sciences* 42, 607–617.
- 40
41
42
43 767
44 767 Lucassen, F., Dulski, P., Abart, R., Franz, G., Rhede, D., Romer, R.L., 2010.
45 768 Redistribution of HFSE during rutile replacement by titanite. *Contributions to
46 769 Mineralogy and Petrology* 160, 279–295.
- 47
48
49
50 770
51 770 Luvizotto, G.L., Zack, T., 2009. Nb and Zr behavior in rutile during high-grade
52 771 metamorphism and retrogression: an example from the Ivrea-Verbano Zone.
53 772 *Chemical Geology* 261, 303–317.
- 54
55
56 773
57 773 Malaspina, N., Hermann, J., Scambelluri, M., Compagnoni, R., 2006. Multistage
58 774 metasomatism in ultrahigh-pressure mafic rocks from the North Dabie Complex
59 775 (China). *Lithos* 90, 19–42.

- 1 776 Maruyama, S., Liou, J.G., Terabayashi, M., 1996. Blueschists and eclogites of the
2 777 world, and their exhumation. *International Geology Review* 38, 485–594.
3
4 778 Meyer, M., John, T., Brandt, S., Klemd, R., 2011. Trace element composition of rutile
5 779 and the application of Zr-in-rutile thermometry to UHT metamorphism (Epupa
6 780 Complex, NW Namibia). *Lithos* 126, 388–401.
7
8 781 Miller, C., Zanetti, A., Thöni, M., 2007. Eclogitisation of gabbroic rocks:
9 782 redistribution of trace elements and Zr in rutile thermometry in an Eo-Alpine
10 783 subduction zone (Eastern Alps). *Chemical Geology* 239, 96–123.
11
12 784 Möller, A., O'Brien, P.J., Kennedy, A., Kröner, A., 2002. Polyphase zircon in
13 785 ultrahigh-temperature granulites (Rogaland, SW Norway): constraints for Pb
14 786 diffusion in zircon. *Journal of Metamorphic Geology* 20, 727–740.
15
16 787 Moraes, R., Brown, M., Fuck, R.A., Camargo, M.A., Lima, T.M., 2002.
17 788 Characterization and P-T evolution of melt-bearing ultrahigh-temperature
18 789 granulites: an Example from the Anápolis–Itaçu Complex of the Brasília Fold
19 790 Belt, Brazil. *Journal of Petrology* 43, 1673–1705.
20
21 791 Morimoto, N., Ferguson, A.K., Ginzburg, I.V., Ross, M., Seifert, F.A., Seifert, J.,
22 792 Seifert, Z., Aoki, K., Gottardi, G., 1988. Nomenclature of pyroxenes. *American*
23 793 *Mineralogist* 73, 1123–1133.
24
25 794 Mosenfelder, J.L., Schertl, H.P., Smyth, J.R., Liou, J.G., 2005. Factors in the
26 795 preservation of coesite: The importance of fluid infiltration. *American*
27 796 *Mineralogist* 90, 779–789.
28
29 797 Okay, A.I., Xu, S., Sengör, A.M.C., 1989. Coesite from the Dabie Shan eclogites,
30 798 central China. *European Journal of Mineralogy* 1, 595–598.
31
32 799 Okay, A.I., 1993. Petrology of a diamond and coesite-bearing metamorphic terrain:
33 800 Dabie Shan, China. *European Journal of Mineralogy* 5, 659–675.
34
35 801 Okay, A.I., Sengör, A.M.C., Satir, M., 1993. Tectonics of an ultrahigh-pressure
36 802 metamorphic terrane: the Dabie Shan/Tongbai orogen, China. *Tectonics* 12,
37 803 1320–1334.
38
39 804 Page, F.Z., Fu, B., Kita, N.T., Fournelle, J., Spicuzza, M.J., Schulze, D.J., Viljoen, F.,
40 805 Basei, M.A.S., Valley, J.W., 2007. Zircons from kimberlite: new insights from
41
42
43
44
45
46
47
48
49
50
51
52
53
54
55
56
57
58
59
60
61
62
63
64
65

1 806 oxygen isotopes, trace element, and Ti in zircon thermometry. *Geochimica et*
2 807 *Cosmochimica Acta* 71, 3887–3903.
3
4 808 Raheim, A., Green, D.H., 1974. Experimental determination of the temperature and
5
6 809 pressure dependence of the Fe-Mg partition coefficient for coexisting garnet and
7
8 810 clinopyroxene. *Contributions to Mineralogy and Petrology* 48, 179–203.
9
10 811 Raith, M., Karmakar, S., Brown, M., 1997. Ultra-high-temperature metamorphism
11
12 812 and multi-stage decompressional evolution of sapphirine granulites from the Palni
13
14 813 hill ranges, southern India. *Journal of Metamorphic Geology* 15, 379–399.
15
16 814 Rolfo, F., Compagnoni, R., Wu, W., Xu, S., 2004. A coherent lithostratigraphic unit in
17
18 815 the coesite-eclogite complex of Dabie Shan, China: geologic and petrologic
19
20 816 evidence. *Lithos* 73, 71–94.
21
22 817 Rowley, D.B., Xue, F., Tucker, R.D., Peng, Z.X., Baker, J., Davis, A., 1997. Ages of
23
24 818 ultrahigh pressure metamorphism and protolith orthogneisses from the eastern
25
26 819 Dabie Shan: U/Pb zircon geochronology. *Earth and Planetary Science Letters* 151,
27
28 820 191–203.
29
30 821 Rubatto, D., Gebauer, D., Compagnoni, R., 1999. Dating of eclogite-facies zircons:
31
32 822 the age of Alpine metamorphism in the Sesia-Lanzo zone (western Alps). *Earth*
33
34 823 *and Planetary Science Letters* 167, 141–158.
35
36 824 Santosh, M., Kusky, T., 2010. Origin of paired high pressure–ultrahigh-temperature
37
38 825 orogens: a ridge subduction and slab window model. *Terra Nova* 22, 35–42.
39
40 826 Spear, F.S., Wark, D.A., Cheney, J.T., Schumacher, J.C., Watson, E.B., 2006.
41
42 827 Zr-in-rutile thermometry in blueschists from Sifnos, Greece. *Contributions to*
43
44 828 *Mineralogy and Petrology* 152, 375–385.
45
46 829 Timms, N.E., Kinny, P.D., Reddy, S.M., Evans, K., Clark, C., Healy, D., 2011.
47
48 830 Relationship among titanium, rare earth elements, U–Pb ages and deformation
49
50 831 microstructures in zircon: Implications for Ti-in-zircon thermometry. *Chemical*
51
52 832 *Geology* 280, 33–46.
53
54 833 Tomkins, H.S., Powell, R., Ellis, D.J., 2007. The pressure dependence of the
55
56 834 zirconium-in-rutile thermometer. *Journal of Metamorphic Geology* 25, 703–713.
57
58 835 Triebold S, von Eynatten H, Luvizotto G L, Zack T (2007) Deducing source rock
59
60
61
62
63
64
65

- 1 836 lithology from detrital rutile geochemistry: an example from the Erzgebirge,
2 837 Germany. *Chemical Geology* 244, 421–436.
- 3
4 838 Triebold, S., Luvizotto, G.L., Tolosana-Delgado, R., Zack, T., von Eynatten, H., 2011.
5
6 839 Discrimination of TiO₂ polymorphs in sedimentary and metamorphic rocks.
7
8 840 *Contributions to Mineralogy and Petrology* 161, 581–596.
- 9
10 841 Wang, S., Li, S., An, S., Hou, Z., 2012. A granulite record of multistage
11
12 842 metamorphism and REE behavior in the Dabie orogen: Constraints from zircon
13
14 843 and rock-forming minerals. *Lithos* 136–139, 109–125.
- 15
16 844 Wang, X., Liou, J.G., Mao, H.K., 1989. Coesite -bearing eclogites from the Dabie
17
18 845 Mountains in central China. *Geology* 17, 1085–1088.
- 19
20 846 Watson, E.B., Harrison, T.M., 2005. Zircon thermometer reveals minimum melting
21
22 847 conditions on earliest earth. *Science* 308, 841–844.
- 23
24 848 Watson, E.B., Wark, D.A., Thomas, J.B., 2006. Crystallization thermometers for
25
26 849 zircon and rutile. *Contributions to Mineralogy and Petrology* 151, 413–433.
- 27
28 850 Wells, R.A., 1977. Pyroxene thermometry in simple and complex systems.
29
30 851 *Contributions to Mineralogy and Petrology* 62, 129–139.
- 31
32 852 Whitehouse, M.J., Platt, J.P., 2003. Dating high-grade metamorphism—constraints
33
34 853 from rare-earth elements in zircons and garnet. *Contributions to Mineralogy and*
35
36 854 *Petrology* 145, 61–74.
- 37
38 855 Whittington, A.G., Hofmeister, A.M., Nabelek, P.I., 2009. Temperature dependent
39
40 856 thermal diffusivity of the Earth's crust and implications for magmatism. *Nature*
41
42 857 458, 319–321.
- 43
44 858 Williams, I.S., Buick, I.S., Cartwright, I., 1996. An extended episode of early
45
46 859 Mesoproterozoic metamorphic fluid flow in the Reynolds Range, central Australia.
47
48 860 *Journal of Metamorphic Geology* 14, 29–47.
- 49
50 861 Whitney, D.L., Evans, B.W., 2010. Abbreviations for names of rock-forming minerals.
51
52 862 *American Mineralogist* 95, 185–187.
- 53
54 863 Wood, B.J., Banno, S., 1973. Garnet-orthopyroxene and orthopyroxene-clinopyroxene
55
56 864 relationship in simple and complex systems. *Contributions to Mineralogy and*
57
58
59
60
61
62
63
64
65

- 1 865 Petrology 42, 109–124.
- 2 866 Wood, B.J., 1974. The solubility of alumina in orthopyroxene coexisting with garnet.
- 3 867 Contributions to Mineralogy and Petrology 46, 1–15.
- 4 868 Wu, Y.B., Zheng, Y., Gao, S., Jiao, W., Liu, Y., 2008. Zircon U–Pb age and trace
- 5 869 element evidence for Paleoproterozoic granulite-facies metamorphism and
- 6 870 Archean crustal rocks in the Dabie Orogen. Lithos 101, 308–322.
- 7 871 Xiao, Y., Hoefs, J., van den Kerkhof, A.M., Li, S., 2001. Geochemical constraints of
- 8 872 the eclogite and granulite facies metamorphism as recognized in the Raobazhai
- 9 873 complex from North Dabie Shan, China. Journal of Metamorphic Geology 19,
- 10 874 3–19.
- 11 875 Xie, Z., Chen, J., Cui, Y., 2010. Episodic growth of zircon in UHP orthogneisses from
- 12 876 the North Dabie Terrane of east-central China: implications for crustal architecture
- 13 877 of a collisional orogen. Journal of Metamorphic Geology 28, 979–995.
- 14 878 Xu, S., Okay, A.I., Ji, S., Sengör, A.M.C., Su, W., Liu, Y.-C., Jiang, L., 1992.
- 15 879 Diamond from the Dabie Shan metamorphic rocks and its implication for tectonic
- 16 880 setting. Science 256, 80–82.
- 17 881 Xu, S., Liu, Y.-C., Su, W., Wang, R., Jiang, L., Wu, W., 2000. Discovery of the
- 18 882 eclogite and its petrography in the Northern Dabie Mountain. Chinese Science
- 19 883 Bulletin 45, 273–278.
- 20 884 Xu, S., Liu, Y.-C., Chen, G., Compagnoni, R., Rolfo, F., He, M., Liu, H., 2003. New
- 21 885 finding of micro-diamonds in eclogites from Dabie-Sulu region in central-eastern
- 22 886 China. Chinese Science Bulletin 48, 988–994.
- 23 887 Xu, S., Liu, Y.-C., Chen, G., Ji, S., Ni, P., Xiao, W., 2005. Microdiamonds, their
- 24 888 classification and tectonic implications for the host eclogites from the Dabie and
- 25 889 Su-Lu regions in central eastern China. Mineralogical Magazine 69, 509–520.
- 26 890 Yuan, H.L., Gao, S., Liu, X.M., Li, H.M., Gunther, D., Wu, F.Y., 2004. Accurate U–Pb
- 27 891 age and trace element determinations of zircon by laser ablation-inductively
- 28 892 coupled plasma mass spectrometry. Geostandards and Geoanalytical Research 28,
- 29 893 353–370.
- 30 894 Zack, T., Moraes, R., Kronz, A., 2004. Temperature dependence of Zr in rutile:

1 895 empirical calibration of a rutile thermometer. *Contributions to Mineralogy and*
2 896 *Petrology* 148, 471–488.
3
4 897 Zack, T., Luvizotto, G.L., 2006. Application of rutile thermometry to eclogites.
5
6 898 *Mineralogy and Petrology* 88, 69–85.
7
8 899 Zhang, G.B., Ellis, D.J., Christy, A.G., Zhang, L.F., Song, S.G., 2010. Zr-in-rutile
9
10 900 thermometry in HP/UHP eclogites from Western China. *Contributions to*
11
12 901 *Mineralogy and Petrology* 160, 427–439.
13
14 902 Zheng, Y.F., Gao, X., Chen, R., Gao, T., 2011. Zr-in-rutile thermometry of eclogite in
15
16 903 the Dabie orogen: Constraints on rutile growth during continental subduction-zone
17
18 904 metamorphism. *Journal of Asian Earth Sciences* 40, 427–451.
19
20
21 905
22
23 906
24
25
26
27
28
29
30
31
32
33
34
35
36
37
38
39
40
41
42
43
44
45
46
47
48
49
50
51
52
53
54
55
56
57
58
59
60
61
62
63
64
65

Figure captions

907

908 **Figure 1** Schematic geological map of the Dabie orogen, with inset showing its
909 location within the Triassic Qinling—Dabie—Sulu collision orogen in central China.
910 Sample localities with sample numbers are described in detail in the text. BZ,
911 Beihuaiyang zone; NDZ, North Dabie complex zone; CDZ, Central Dabie UHP
912 metamorphic zone; SDZ, South Dabie low-*T* eclogite zone; SZ, Susong complex zone;
913 HMZ, Huwan mélangé zone; HZ, Hong'an low-*T* eclogite zone; DC,
914 amphibolite-facies Dabie complex; XMF, Xiaotian-Mozitan fault; WSF,
915 Wuhe-Shuihou fault; HMF, Hualiangting-Mituo fault; TSF, Taihu-Shanlong fault; TLF,
916 Tan-Lu fault; SMF, Shangcheng-Macheng fault.

917

918 **Figure 2** Photomicrographs of eclogite (sample 07LT6-1) from the Luotian dome in
919 the Dabie orogen. a. Omphacite (Omp) and quartz (Qtz) inclusions in garnet with two
920 generations of symplectites (Hy+Di+Pl and Hbl+Pl+Mt); b. Omphacite, rutile and
921 quartz inclusions in garnet, rimmed by distinctive double symplectites (Liu et al.
922 2011b); c. Quartz and rutile inclusions in garnet with well-developed radial cracks
923 (Liu et al. 2011b); d. Clinopyroxene (Cpx) + plagioclase (Pl) + quartz (Qtz)
924 intergrowth after omphacite in garnet. Mineral abbreviations are after Whitney and
925 Evans (2010).

926

927 **Figure 3** Cathodoluminescence (CL) (a, c, e, g and i–k) and Back scattered electron
928 (BSE) images (b, d, f, h and l) for zircon from sample 07LT6-1. Zircon (a) and (b), (c)
929 and (d), (e) and (f), (g) and (h), and (k) and (l) are the same grains, respectively. The
930 open circles are analysis spots with available $^{206}\text{Pb}/^{238}\text{U}$ ages. Omp represents low-Na
931 omphacite as mentioned in the text.

932

933 **Figure 4** WEF–Jd–Ae diagram (after Morimoto et al. 1988) of clinopyroxenes
934 occurring as inclusions in garnet and zircon of the eclogite (sample 07LT6-1) from the
935 Luotian dome.

936

937 **Figure 5** Representative Raman spectra of mineral inclusions in zircon of eclogites
938 from the Luotian dome. (a) Omphacite and quartz; (b) Rutile; (c) Garnet. These
939 spectra also contain host zircon peaks at 227–228, 357–359, 440–441, 975–976 and
940 1009–1010 cm^{-1} .

941

942 **Figure 6** Calculated Zr temperatures ($^{\circ}\text{C}$) of rutile occurring as inclusions in garnet
943 (a), in zircon inner mantle (b), in zircon outer mantle (c) and in zircon rim (d) from
944 the investigated samples in the North Dabie complex zone.

945

946 **Figure 7** Diagram of Zr-in-rutile temperatures ($^{\circ}\text{C}$) estimated at the inferred
947 metamorphic pressures (GPa) for the eclogites from the Luotian dome. Red circles,
948 black circles and black triangles represent calculated temperatures from inner mantle
949 (M1), outer mantle (M2) and rim domains of zircon, respectively (see explanation in
950 the text).

951

952 **Figure 8** Diagram of zircon U-Pb age (Ma) and corresponding Ti-in-zircon
953 temperatures ($^{\circ}\text{C}$) for the Type 1 eclogites from the Luotian dome. Square, circle and
954 triangle symbols represent calculated temperatures from samples 03LT1-1, 06LT3-2
955 and 07LT6-1, respectively. Blue, red, purple, green and gray symbols denote different
956 groups of metamorphic zircon domains formed at 230–240 Ma (pre-peak mantle),
957 220–230 Ma (UHP eclogite-facies inner mantle M1), 210–220 Ma (HP eclogite-facies
958 outer mantle M2), 200–210 Ma (granulite-facies rim) and 180–200 Ma
959 (amphibolites-facies rim), respectively (see explanation in the text).

960

961 **Figure 9** Diagram of zircon U-Pb age (Ma) and corresponding Ti-in-zircon
962 temperatures ($^{\circ}\text{C}$) for the Type 2 eclogites (samples LT9 and LT10) from the Luotian
963 dome. Black square and red circle symbols refer to the Neoproterozoic magmatic and
964 metamorphic zircon cores dated by Liu et al. (2007a).

965

1
2
3
4
5
6
7
8
9
10
11
12
13
14
15
16
17
18
19
20
21
22
23
24
25
26
27
28
29
30
31
32
33
34
35
36
37
38
39
40
41
42
43
44
45
46
47
48
49
50
51
52
53
54
55
56
57
58
59
60
61
62
63
64
65

966 **Figure 10** A schematic P - T - t path for the eclogites from the Luotian dome in the
967 Dabie orogen. The equilibrium lines for diamond = graphite (Kennedy and Kennedy,
968 1976) and coesite = quartz (Hemingway et al., 1998) are shown.

Table 1 Electron microprobe analyses of representative minerals from the eclogite (sample 07LT6-1) in the Luotian dome (wt%)

| Mineral | Garnet | | High-Na omphacite | | | | Low-Na omphacite | | | |
|------------------------------------|--------|--------|-------------------|-------|-------|-------|------------------|-------|-------|--------|
| | No. | Gt1 | Gt1a | Omp4 | Omp1 | Omp2 | Omp3 | Cpx1 | Cpx4 | Cpx5 |
| Site | m | iz | ig | ig | ig | ig | iz | iz | iz | iz |
| SiO₂ | 38.01 | 39.44 | 55.58 | 55.49 | 54.34 | 54.41 | 55.20 | 54.93 | 53.35 | 56.77 |
| TiO₂ | 0.10 | 0.03 | 0.03 | 0.06 | 0.05 | 0.10 | 0.04 | 0.04 | 0.00 | 0.00 |
| Al₂O₃ | 21.02 | 22.00 | 10.07 | 10.48 | 10.71 | 10.26 | 7.64 | 6.18 | 8.90 | 8.36 |
| FeO | 26.89 | 23.50 | 7.04 | 6.71 | 7.35 | 7.12 | 5.74 | 6.53 | 5.47 | 5.74 |
| Cr₂O₃ | 0.19 | 0.00 | 0.00 | 0.04 | 0.10 | 0.00 | 0.02 | 0.05 | 0.03 | 0.00 |
| MnO | 0.24 | 0.82 | 0.01 | 0.03 | 0.08 | 0.06 | 0.15 | 0.05 | 0.03 | 0.14 |
| MgO | 3.82 | 6.52 | 7.93 | 7.84 | 7.44 | 8.05 | 10.43 | 11.40 | 10.15 | 10.63 |
| CaO | 9.88 | 8.12 | 12.71 | 12.88 | 13.14 | 13.76 | 17.30 | 17.81 | 19.14 | 15.05 |
| Na₂O | 0.06 | 0.00 | 6.62 | 6.33 | 6.44 | 6.09 | 3.43 | 2.98 | 2.41 | 3.89 |
| K₂O | 0.00 | 0.00 | 0.00 | 0.02 | 0.00 | 0.00 | 0.00 | 0.00 | 0.00 | 0.00 |
| Total | 100.02 | 100.43 | 99.99 | 99.88 | 99.65 | 99.85 | 99.95 | 99.97 | 99.48 | 100.62 |
| O | 12 | 12 | 6 | 6 | 6 | 6 | 6 | 6 | 6 | 6 |
| Si | 2.979 | 3.030 | 1.992 | 1.994 | 1.959 | 1.959 | 2.009 | 2.004 | 1.962 | 2.044 |
| Al^{IV} | 0.021 | 0.000 | 0.008 | 0.006 | 0.041 | 0.041 | 0.000 | 0.000 | 0.038 | 0.000 |
| Al^{VI} | 1.919 | 1.990 | 0.416 | 0.437 | 0.414 | 0.393 | 0.327 | 0.266 | 0.347 | 0.335 |
| Fe³⁺ | 0.088 | 0.075 | 0.049 | 0.005 | 0.070 | 0.066 | 0.000 | 0.000 | 0.000 | 0.000 |
| Ti | 0.006 | 0.002 | 0.001 | 0.002 | 0.001 | 0.003 | 0.001 | 0.001 | 0.000 | 0.000 |
| Fe²⁺ | 1.674 | 1.434 | 0.162 | 0.196 | 0.152 | 0.147 | 0.175 | 0.199 | 0.168 | 0.099 |
| Cr | 0.012 | 0.000 | 0.000 | 0.001 | 0.003 | 0.000 | 0.001 | 0.001 | 0.001 | 0.000 |
| Mg | 0.446 | 0.747 | 0.424 | 0.420 | 0.400 | 0.432 | 0.566 | 0.620 | 0.556 | 0.571 |
| Mn | 0.016 | 0.053 | 0.000 | 0.001 | 0.002 | 0.002 | 0.005 | 0.002 | 0.001 | 0.004 |
| Ca | 0.830 | 0.668 | 0.488 | 0.496 | 0.508 | 0.531 | 0.675 | 0.696 | 0.754 | 0.581 |
| Na | 0.009 | 0.000 | 0.460 | 0.441 | 0.450 | 0.425 | 0.242 | 0.211 | 0.172 | 0.272 |
| K | 0.000 | 0.000 | 0.000 | 0.001 | 0.000 | 0.000 | 0.000 | 0.000 | 0.000 | 0.000 |

Note: m, matrix; ig, inclusion in garnet; iz, inclusion in zircon. Garnet/omphacite stoichiometries and the amount of Fe³⁺ and Fe²⁺ were estimated on the base of eight/four cations and the charge-balance constraint.

Table 2

Table 2 Major element compositions and Zr temperatures of rutile inclusions in zircon and zircon U-Pb ages for eclogites from the Luotian dome in the North Dabie complex zone

| Analysis No. | Locality | SiO ₂ | Al ₂ O ₃ | TiO ₂ | FeO | Cr ₂ O ₃ | Nb ₂ O ₅ | ZrO ₂ | Total | Zr(ppm) | T(°C) | ²⁰⁶ Pb/ ²³⁸ U Age(Ma) |
|----------------|----------|------------------|--------------------------------|------------------|------|--------------------------------|--------------------------------|------------------|-------|---------|-------|--|
| 03LT1-1 | | | | | | | | | | | | |
| 03LT1-1Rt1 | M2 | 0.00 | 0.00 | 96.65 | 0.36 | 0.04 | 0.06 | 0.19 | 97.29 | 1421 | 844 | 214±3 |
| 03LT1-1Rt1a | M2 | 0.00 | 0.00 | 97.21 | 0.35 | 0.04 | 0.03 | 0.16 | 97.79 | 1199 | 825 | 214±3 |
| 03LT1-1Rt4 | M1 | 0.00 | 0.00 | 97.41 | 0.49 | 0.04 | 0.05 | 0.33 | 98.31 | 2419 | 988 | |
| 03LT1-1Rt4a | M2 | 0.00 | 0.00 | 97.98 | 0.52 | 0.04 | 0.06 | 0.35 | 98.94 | 2560 | 915 | |
| 03LT1-1Rt4b | M2 | 0.00 | 0.00 | 98.27 | 0.47 | 0.03 | 0.07 | 0.34 | 99.19 | 2538 | 913 | |
| 03LT1-1Rt5 | M2 | 0.00 | 0.00 | 98.00 | 0.25 | 0.03 | 0.08 | 0.31 | 98.68 | 2301 | 901 | |
| 03LT1-1Rt1 | M2 | 0.00 | 0.00 | 98.33 | 0.33 | 0.04 | 0.07 | 0.11 | 98.89 | 843 | 788 | |
| 03LT1-1Rt6 | M2 | 0.00 | 0.00 | 97.56 | 0.54 | 0.04 | 0.08 | 0.73 | 98.95 | 5416 | 1018 | |
| 03LT1-1Rt9 | M2 | 0.00 | 0.00 | 98.51 | 0.47 | 0.03 | 0.08 | 0.14 | 99.23 | 1014 | 807 | |
| 03LT1-1Rt6a | M2 | 0.00 | 0.00 | 97.68 | 0.56 | 0.03 | 0.05 | 0.22 | 98.53 | 1591 | 857 | |
| 03LT1-1Rt9 | M2 | 0.00 | 0.00 | 96.61 | 2.60 | 0.03 | 0.05 | 0.11 | 99.40 | 814 | 785 | |
| 03LT1-1Rt2 | M1 | 0.07 | 0.00 | 98.39 | 0.45 | 0.08 | 0.09 | 0.34 | 99.43 | 2515 | 993 | |
| 03LT1-1Rt3 | M1 | 0.04 | 0.00 | 99.35 | 0.36 | 0.07 | 0.06 | 0.22 | 100.1 | 1628 | 936 | |
| 03LT1-1Rt7 | M2 | 0.04 | 0.00 | 98.11 | 0.53 | 0.07 | 0.06 | 0.15 | 98.96 | 1110 | 817 | |
| 03LT1-1Rt8 | M2 | 0.05 | 0.00 | 98.77 | 0.53 | 0.07 | 0.07 | 0.37 | 99.86 | 2737 | 923 | |
| 03LT1-1Rt7 | M2 | 0.05 | 0.00 | 98.36 | 0.26 | 0.06 | 0.07 | 0.30 | 99.10 | 2220 | 897 | |
| 03LT1-1Rt1b | M2 | 0.05 | 0.00 | 98.38 | 0.44 | 0.04 | 0.09 | 0.15 | 99.16 | 1131 | 819 | |
| 03LT1-1ARt2 | M1 | 0.04 | 0.00 | 97.98 | 0.37 | 0.02 | 0.07 | 0.23 | 98.72 | 1702 | 941 | |
| 03LT1-1ARt3 | M1 | 0.05 | 0.00 | 97.53 | 0.48 | 0.04 | 0.07 | 0.38 | 98.55 | 2800 | 1008 | |
| 03LT1-1ARt1 | M2 | 0.06 | 0.00 | 98.18 | 0.37 | 0.07 | 0.09 | 0.18 | 98.95 | 1332 | 837 | |
| 06LT3-2 | | | | | | | | | | | | |
| 06LT3-2Rt2 | M2 | 0.00 | 0.00 | 98.19 | 0.14 | 0.03 | 0.01 | 0.15 | 98.51 | 1080 | 814 | |
| 06LT3-2Rt3 | M1 | 0.00 | 0.00 | 97.46 | 0.39 | 0.02 | 0.01 | 0.25 | 98.13 | 1864 | 954 | |
| 06LT3-2Rt4 | M2 | 0.00 | 0.00 | 97.40 | 0.22 | 0.02 | 0.02 | 0.78 | 98.43 | 5771 | 1028 | |
| 06LT3-2Rt5 | rim | 0.04 | 0.00 | 98.41 | 0.21 | 0.02 | 0.00 | 0.28 | 98.97 | 2098 | 838 | 200±18 |
| 06LT3-2Rt5a | rim | 0.04 | 0.00 | 98.09 | 0.20 | 0.05 | 0.01 | 0.32 | 98.72 | 2368 | 852 | 200±18 |
| 06LT3-2Rt1 | M2 | 0.05 | 0.00 | 97.92 | 0.15 | 0.06 | 0.01 | 0.18 | 98.37 | 1332 | 837 | |
| 06LT3-2Rt2a | M2 | 0.03 | 0.00 | 97.89 | 0.15 | 0.02 | 0.01 | 0.16 | 98.27 | 1202 | 826 | |
| 07LT6-1 | | | | | | | | | | | | |
| 07LT6-1Rt1 | M1 | 0.03 | 0.00 | 98.69 | 0.48 | 0.02 | 0.04 | 0.14 | 99.41 | 1033 | 881 | 221±6 |
| 07LT6-1Rt2 | M1 | 0.04 | 0.00 | 98.22 | 0.63 | 0.01 | 0.03 | 0.24 | 99.17 | 1790 | 948 | 228±5 |
| 07LT6-1Rt3 | M1 | 0.05 | 0.00 | 98.13 | 0.48 | 0.05 | 0.03 | 0.33 | 99.06 | 2405 | 987 | |
| 07LT6-1Rt4 | M1 | 0.04 | 0.00 | 98.57 | 0.40 | 0.03 | 0.04 | 0.26 | 99.34 | 1955 | 959 | |
| 07LT6-1Rt5 | M2 | 0.06 | 0.00 | 98.34 | 0.52 | 0.02 | 0.04 | 0.27 | 99.25 | 1978 | 883 | |

| | | | | | | | | | | | | |
|--------------|----|------|------|-------|------|------|------|------|-------|------|------|-------|
| 07LT6-1Rt6 | M2 | 0.06 | 0.00 | 98.07 | 0.47 | 0.02 | 0.04 | 0.40 | 99.06 | 2983 | 934 | |
| 07LT6-1Rt7 | M2 | 0.06 | 0.00 | 98.50 | 0.49 | 0.03 | 0.04 | 0.20 | 99.32 | 1458 | 847 | |
| 07LT6-1Rt8 | M2 | 0.03 | 0.00 | 98.68 | 0.55 | 0.02 | 0.00 | 0.22 | 99.51 | 1627 | 860 | |
| 07LT6-1Rt9 | M2 | 0.07 | 0.00 | 98.67 | 0.52 | 0.03 | 0.16 | 0.29 | 99.75 | 2163 | 894 | |
| 07LT6-1Rt10 | M2 | 0.06 | 0.00 | 98.56 | 0.45 | 0.03 | 0.04 | 0.17 | 99.32 | 1286 | 833 | |
| 07LT6-1Rt11 | M2 | 0.06 | 0.00 | 98.57 | 0.50 | 0.03 | 0.04 | 0.25 | 99.44 | 1876 | 876 | |
| 07LT6-1Rt12 | M1 | 0.05 | 0.00 | 98.33 | 0.46 | 0.03 | 0.04 | 0.25 | 99.16 | 1819 | 950 | |
| 07LT6-1Rt13 | M2 | 0.04 | 0.00 | 98.59 | 0.36 | 0.02 | 0.01 | 0.29 | 99.30 | 2133 | 892 | |
| 07LT6-1Rt14 | M2 | 0.06 | 0.00 | 98.57 | 0.41 | 0.02 | 0.03 | 0.21 | 99.30 | 1520 | 852 | |
| 07LT6-1Rt15 | M1 | 0.07 | 0.00 | 98.18 | 0.46 | 0.02 | 0.00 | 0.26 | 98.99 | 1929 | 957 | 226±7 |
| 07LT6-1Rt16 | M1 | 0.06 | 0.00 | 98.17 | 0.46 | 0.02 | 0.00 | 0.34 | 99.05 | 2495 | 992 | 228±7 |
| 07LT6-1Rt17 | M2 | 0.08 | 0.00 | 97.76 | 0.44 | 0.04 | 0.05 | 0.45 | 98.82 | 3297 | 948 | |
| 07LT6-1Rt18 | M2 | 0.07 | 0.00 | 98.61 | 0.11 | 0.01 | 0.02 | 0.25 | 99.08 | 1831 | 873 | |
| 07LT6-1Rt19 | M2 | 0.05 | 0.00 | 97.65 | 0.46 | 0.03 | 0.04 | 0.40 | 98.63 | 2977 | 934 | |
| 07LT6-1Rt20 | M2 | 0.07 | 0.00 | 98.61 | 0.28 | 0.03 | 0.00 | 0.20 | 99.18 | 1447 | 846 | |
| 07LT6-1Rt1a | M1 | 0.03 | 0.00 | 98.46 | 0.48 | 0.02 | 0.00 | 0.15 | 99.14 | 1078 | 886 | 221±6 |
| 09LT1 | | | | | | | | | | | | |
| 09LT1Rt1 | M1 | 0.03 | 0.00 | 98.43 | 0.41 | 0.03 | 0.00 | 0.33 | 99.24 | 2405 | 987 | |
| 09LT1Rt2 | M1 | 0.21 | 0.00 | 98.15 | 0.32 | 0.02 | 0.03 | 0.58 | 99.32 | 4310 | 1072 | |
| 09LT2 | | | | | | | | | | | | |
| 09LT2Rt2 | M2 | 0.05 | 0.00 | 97.88 | 0.39 | 0.05 | 0.01 | 0.28 | 98.66 | 2072 | 888 | |
| 09LT2Rt1 | M1 | 0.14 | 0.00 | 97.45 | 0.58 | 0.05 | 0.00 | 0.51 | 98.73 | 3773 | 1052 | 224±3 |

Notes: M1, inner mantle; M2, outer mantle. All rutiles in this table are inclusions in zircon, the analysis method was EPMA. Temperatures were calculated by Tomkins *et al.* (2007); the pressures were set to be 4 GPa for M1, 2 GPa for M2 and 1 GPa for rim domains. Age data from Liu *et al.* (2011a) and Gu (2012).

Table 3 Major element compositions and Zr temperatures of rutile inclusions in garnet for eclogites from the Luotian dome in the North Dabie complex zone

| Analysis No. | SiO ₂ | Al ₂ O ₃ | FeO | TiO ₂ | Cr ₂ O ₃ | Nb ₂ O ₅ | ZrO ₂ | Total | Zr (ppm) | Tt (°C)/4GPa | Tt (°C)/2GPa |
|--------------|------------------|--------------------------------|------|------------------|--------------------------------|--------------------------------|------------------|--------|----------|--------------|--------------|
| 07LT6-1-R1 | 0.00 | 0.00 | 0.31 | 100.03 | 0.03 | 0.03 | 0.01 | 100.41 | 67 | 633 | 595 |
| 07LT6-1-R3 | 0.00 | 0.02 | 0.27 | 99.27 | 0.01 | 0.06 | 0.07 | 99.70 | 481 | 799 | 753 |
| 07LT6-1-R2 | 0.00 | 0.02 | 0.32 | 99.21 | 0.02 | 0.05 | 0.03 | 99.66 | 252 | 738 | 695 |
| 07LT6-1-R5 | 0.00 | 0.00 | 0.30 | 99.66 | 0.03 | 0.03 | 0.05 | 100.08 | 363 | 772 | 727 |
| 07LT6-1-R6 | 0.00 | 0.04 | 0.23 | 99.82 | 0.08 | 0.04 | 0.02 | 100.22 | 141 | 690 | 648 |
| 07LT6-1-R7 | 0.00 | 0.02 | 0.23 | 99.41 | 0.05 | 0.04 | 0.02 | 99.77 | 126 | 681 | 640 |
| 07LT6-1A-R1 | 0.00 | 0.00 | 0.29 | 98.23 | 0.06 | 0.04 | 0.05 | 98.66 | 345 | 767 | 723 |
| 07LT6-1A-R2 | 0.00 | 0.00 | 0.21 | 99.35 | 0.10 | 0.02 | 0.03 | 99.71 | 215 | 725 | 682 |
| 07LT6-1A-R3 | 0.00 | 0.00 | 0.43 | 98.90 | 0.05 | 0.04 | 0.03 | 99.44 | 192 | 715 | 673 |
| 07LT6-1A-R4 | 0.00 | 0.00 | 0.35 | 99.26 | 0.03 | 0.04 | 0.01 | 99.69 | 96 | 660 | 620 |
| 07LT6-1A-R5 | 0.00 | 0.00 | 0.30 | 100.52 | 0.03 | 0.03 | 0.10 | 100.97 | 710 | 839 | 792 |
| 07LT6-1A-R6 | 0.00 | 0.02 | 0.15 | 100.81 | 0.21 | 0.05 | 0.07 | 101.30 | 504 | 804 | 758 |
| 07LT6-1A-R7 | 0.00 | 0.00 | 0.21 | 100.35 | 0.07 | 0.11 | 0.11 | 100.85 | 777 | 849 | 801 |
| 07LT6-1-R4 | 0.00 | 0.01 | 0.30 | 101.11 | 0.03 | 0.04 | 0.08 | 101.56 | 561 | 815 | 710 |
| 09LT2-1-R1 | 0.00 | 0.01 | 0.36 | 101.36 | 0.05 | 0.03 | 0.04 | 101.88 | 298 | 754 | 776 |
| 09LT2-1-R2 | 0.00 | 0.01 | 0.50 | 101.52 | 0.03 | 0.07 | 0.08 | 102.20 | 608 | 823 | 625 |
| 09LT2-1-R3 | 0.00 | 0.00 | 0.46 | 100.88 | 0.04 | 0.03 | 0.01 | 101.42 | 102 | 665 | 782 |
| 09LT2-1-R4 | 0.06 | 0.00 | 0.36 | 96.97 | 0.05 | 0.03 | 0.09 | 97.56 | 645 | 829 | 770 |
| 03LT1-1H-R1 | 0.00 | 0.00 | 0.36 | 101.55 | 0.03 | 0.07 | 0.08 | 102.09 | 573 | 817 | 789 |
| 03LT1-1H-R2 | 0.00 | 0.00 | 0.37 | 101.93 | 0.09 | 0.07 | 0.10 | 102.54 | 693 | 837 | 768 |
| 03LT1-1Ru1 | 0.07 | 0.03 | 1.01 | 99.29 | 0.04 | 0.08 | 0.04 | 101.08 | 296 | 753 | 709 |
| 03LT1-1Ru2 | 0.03 | 0.02 | 0.51 | 96.94 | 0.06 | 0.07 | 0.06 | 98.01 | 466 | 796 | 750 |
| 03LT1-1Ru3 | 0.08 | 0.04 | 1.23 | 98.47 | 0.06 | 0.07 | 0.04 | 100.58 | 311 | 758 | 713 |
| 06LT3-2Ru1 | 0.01 | 0.01 | 0.30 | 98.57 | 0.10 | 0.02 | 0.08 | 99.14 | 607 | 823 | 776 |
| 06LT3-2Ru2 | 0.03 | 0.05 | 0.53 | 98.33 | 0.10 | 0.01 | 0.03 | 99.28 | 229 | 730 | 688 |

Temperatures were calculated using the equation given by Tomkins *et al.* (2007), the pressures were set to be 4 GPa and 2 GPa, respectively. The Zr contents were analyzed by EPMA.

Table 4 Ti-in-zircon temperatures and zircon U-Pb ages for eclogites from the Luotian dome in the North Dabie complex zone

| Type | Sample No. | Domain | Nature | Ti (ppm) | T (°C) | $^{206}\text{Pb}/^{238}\text{U}$ Age (Ma) |
|--------------|----------------|--------|--------|----------|--------|---|
| Type 1 | 03LT1-1 | | | | | |
| | 03LT1-1-1-1 | m | me | 3.4 | 654 | 226±4 |
| | 03LT1-1-3-1 | m | me | 3.6 | 659 | 231±4 |
| | 03LT1-1-8-1 | m | me | 4.8 | 680 | 224±3 |
| | 03LT1-1-10-1 | m | me | 3.1 | 647 | 216±3 |
| | 03LT1-1-17-1 | m | me | 4.4 | 673 | 217±4 |
| | 03LT1-1-16-1 | m | me | 3.4 | 654 | 234±3 |
| | 03LT1-1-18-1 | m | me | 2.2 | 622 | 217±4 |
| | 03LT1-1-20-1 | m | me | 8.5 | 726 | 225±3 |
| | 03LT1-1-22-1 | m | me | 4.7 | 678 | 229±3 |
| | 03LT1-1-26-1 | m | me | 4 | 667 | 213±3 |
| | 03LT1-1-24-1 | m | me | 26.9 | 836 | 220±3 |
| | 06LT3-2 | | | | | |
| | 06LT3-2-1-1 | r | me | 4.6 | 678 | 180±12 |
| | 06LT3-2-3-1 | r | me | 3.4 | 653 | 191±10 |
| | 06LT3-2-7-1 | m | me | 2.9 | 643 | 220±3 |
| | 06LT3-2-6-1 | m | me | 63.1 | 934 | 225±14 |
| | 06LT3-2-11-1 | m | me | 6.8 | 709 | 207±5 |
| | 06LT3-2-15-1 | m | me | 13.9 | 771 | 230±25 |
| | 06LT3-2-18-1 | m | me | 20.3 | 807 | 215±18 |
| | 06LT3-2-19-1 | m | me | 97.8 | 991 | 211±3 |
| | 06LT3-2-21-1 | r | me | 25 | 828 | 207±4 |
| | 06LT3-2-20-1 | r | me | 16.2 | 785 | 200±18 |
| | 07LT6-1 | | | | | |
| | 07LT6-1-1-1 | m | me | 4.8 | 680 | 221±6 |
| | 07LT6-1-3-1 | m | me | 5.2 | 688 | 225±5 |
| | 07LT6-1-5-1 | r | me | 3.1 | 647 | 189±6 |
| | 07LT6-1-8-2 | m | me | 20.5 | 808 | 218±5 |
| | 07LT6-1-9-1 | r | me | 3.3 | 652 | 197±5 |
| | 07LT6-1-10-2 | m | me | 4 | 667 | 227±5 |
| | 07LT6-1-17-1 | r | me | 3.3 | 652 | 208±6 |
| | 07LT6-1-13-1 | m | me | 66.3 | 940 | 218±5 |
| | 07LT6-1-15-1 | m | me | 2.9 | 644 | 238±7 |
| 07LT6-1-14-1 | m | me | 3.2 | 649 | 215±7 | |
| 07LT6-1-16-1 | m | me | 2.4 | 630 | 225±5 | |
| LT10 | | | | | | |
| LT10-2-1 | c | ma | 6.9 | 709 | 783±13 | |
| LT10-2-2 | c | ma | 8.8 | 730 | 737±15 | |

| | | | | | | | |
|---------------|-------------------|----|-------|-------|--------|--------|--|
| Type 2 | LT10-3-2 | c | me | 6.4 | 703 | 822±17 | |
| | LT10-4-1 | c | ma | 7.7 | 718 | 638±11 | |
| | LT10-1-1 | c | me | 274 | 1149 | 788±13 | |
| | LT10-1-2 | c | me | 9.3 | 734 | 766±13 | |
| | LT10-4-2 | c | me | 4.3 | 672 | 788±14 | |
| | LT10-3-5 | c | ma | 47.2 | 898 | 799±15 | |
| | LT10-3-9 | c | ma | 6.3 | 702 | 642±14 | |
| | LT10-1-4 | c | me | 48.5 | 902 | 791±13 | |
| | LT10-4-5 | c | ma | 14.1 | 772 | 798±16 | |
| | LT10-4-4 | c | ma | 17.7 | 794 | 784±16 | |
| | LT10-4-7 | c | ma | 6.3 | 702 | 791±16 | |
| | LT10-4-3 | c | me | 12.6 | 762 | 335±7 | |
| | LT10-1-8 | c | me | 21.4 | 812 | 783±13 | |
| | LT10-1-11 | c | me | 5.5 | 691 | 799±14 | |
| | LT10-1-9 | c | me | 33.7 | 860 | 730±12 | |
| | LT10-3-6 | c | me | 6 | 698 | 696±14 | |
| | LT10-3-7 | c | me | 11.5 | 753 | 726±15 | |
| | <i>LT9</i> | | | | | | |
| | LT9-2-1 | c | ma | 17.6 | 793 | 802±16 | |
| | LT9-3-1 | c | me | 236.1 | 1124 | 830±18 | |
| LT9-2-2 | c | ma | 136.2 | 1038 | 736±14 | | |
| LT9-1-6 | c | me | 94.4 | 986 | 375±6 | | |
| LT9-1-7 | c | me | 68.8 | 945 | 707±12 | | |

Notes: c, core; m, mantle; r, rim; ma, magmatic; me, metamorphic. Temperatures were calculated by Watson *et al.* (2006). The Ti contents in zircons were analyzed by LA-MC-ICPMS.

Figure 1
[Click here to download high resolution image](#)

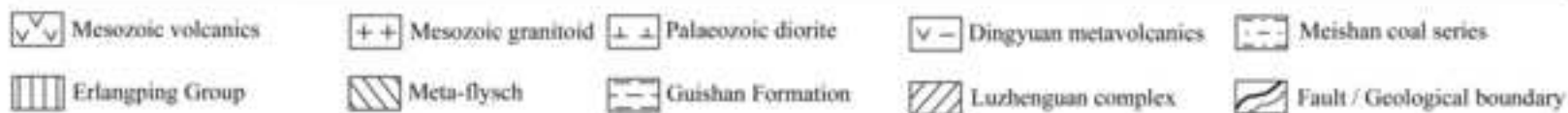
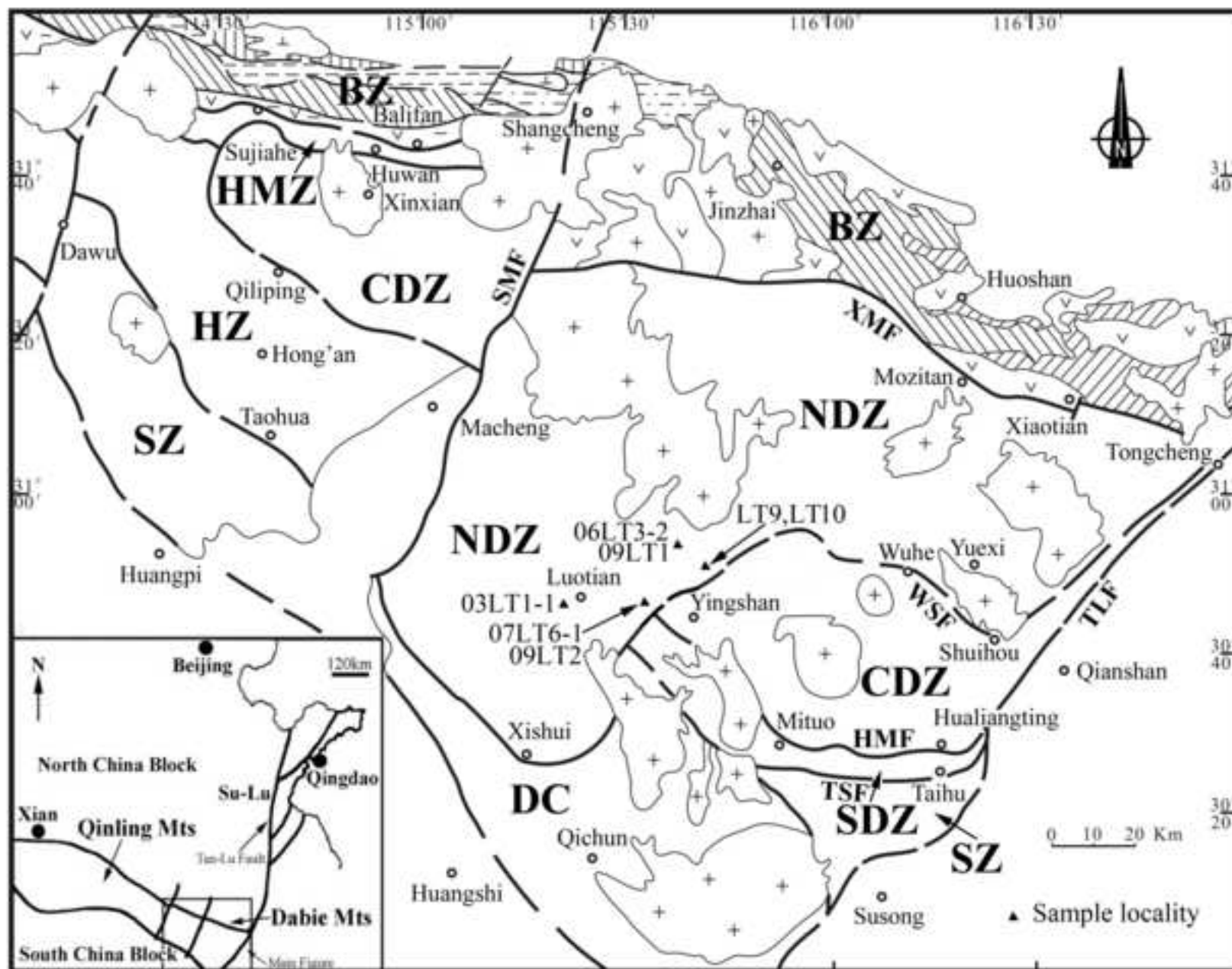


Figure 2
[Click here to download high resolution image](#)

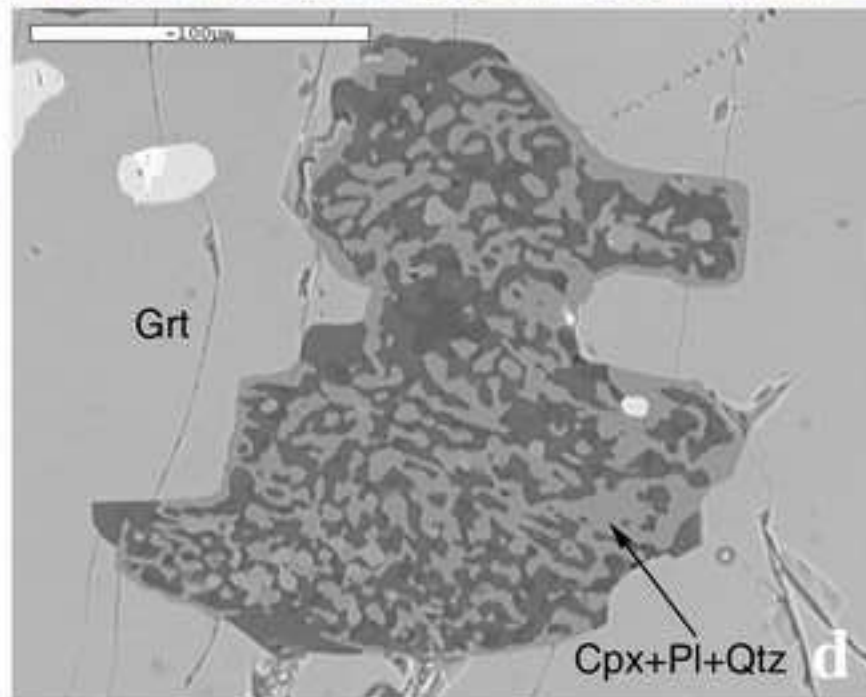
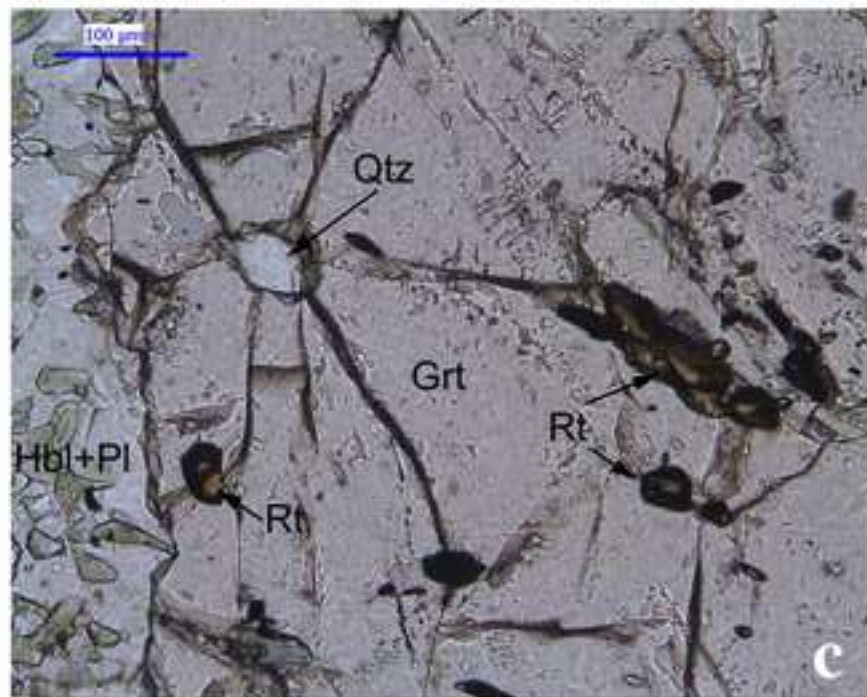
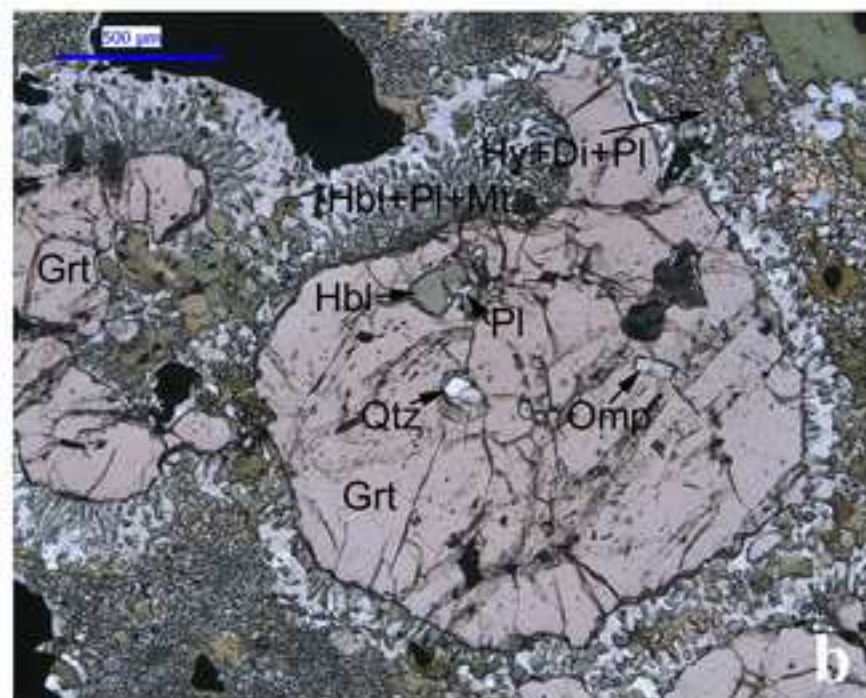
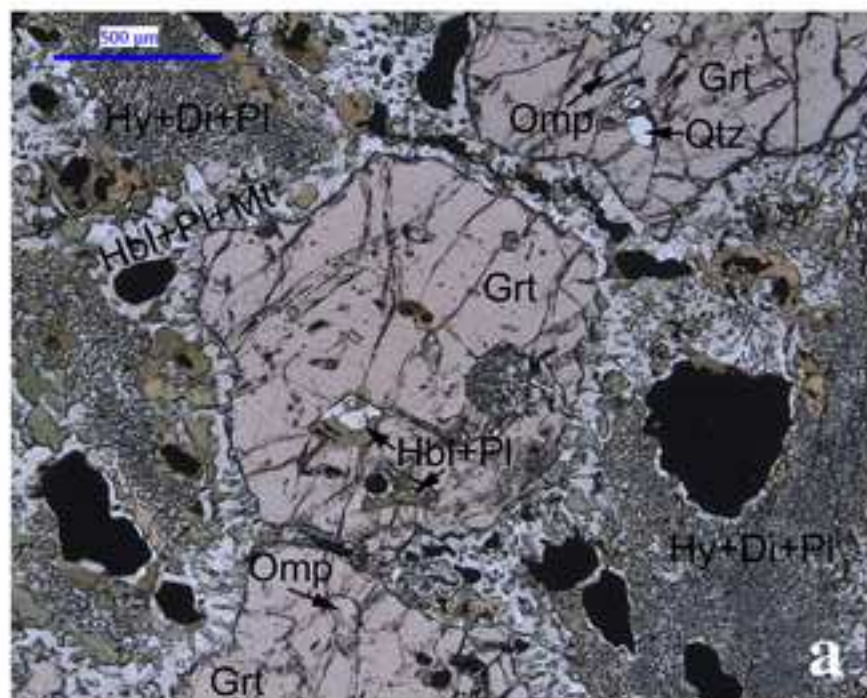


Figure 3
[Click here to download high resolution image](#)

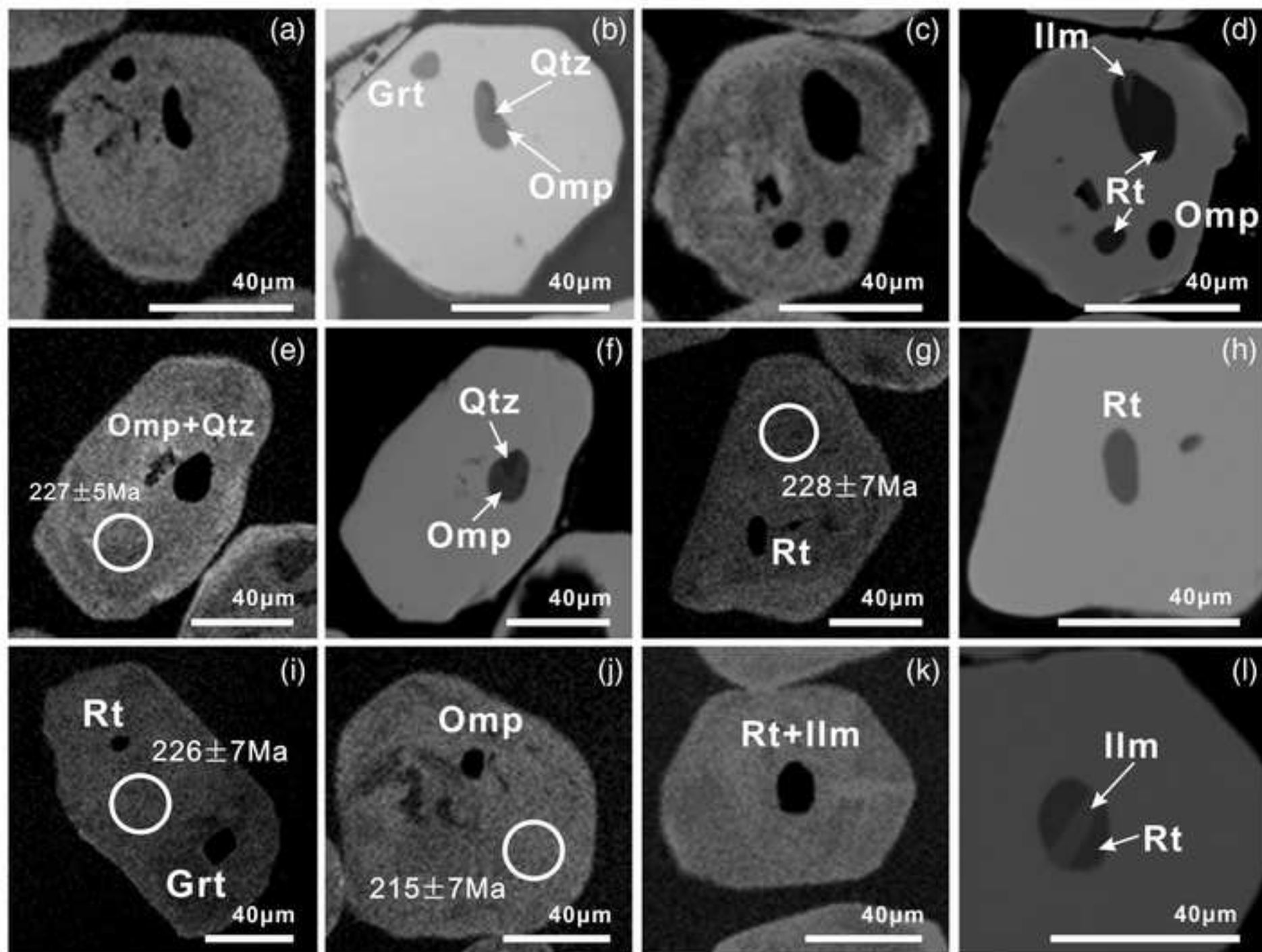


Figure 4
[Click here to download high resolution image](#)

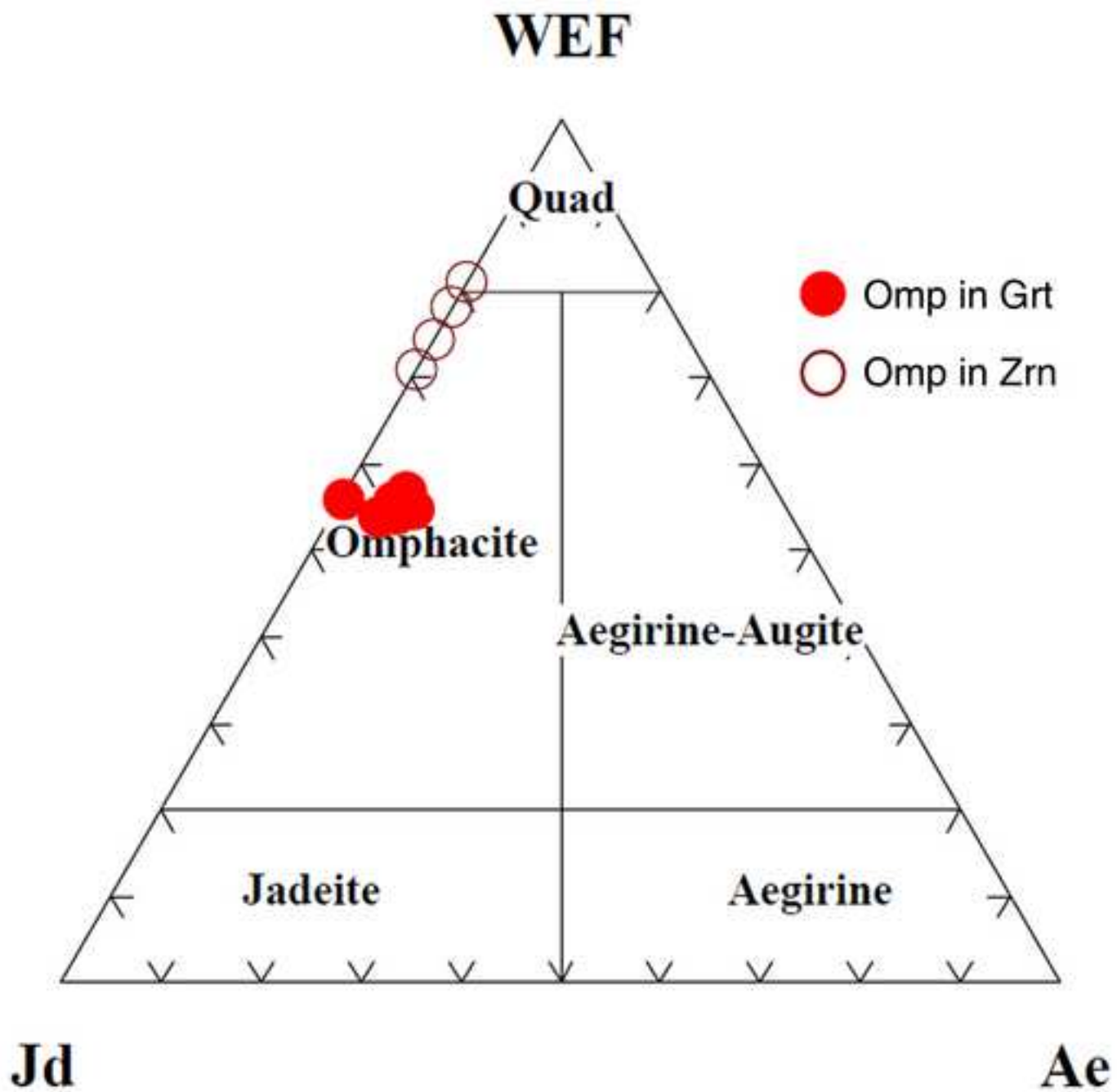


Figure 5
[Click here to download high resolution image](#)

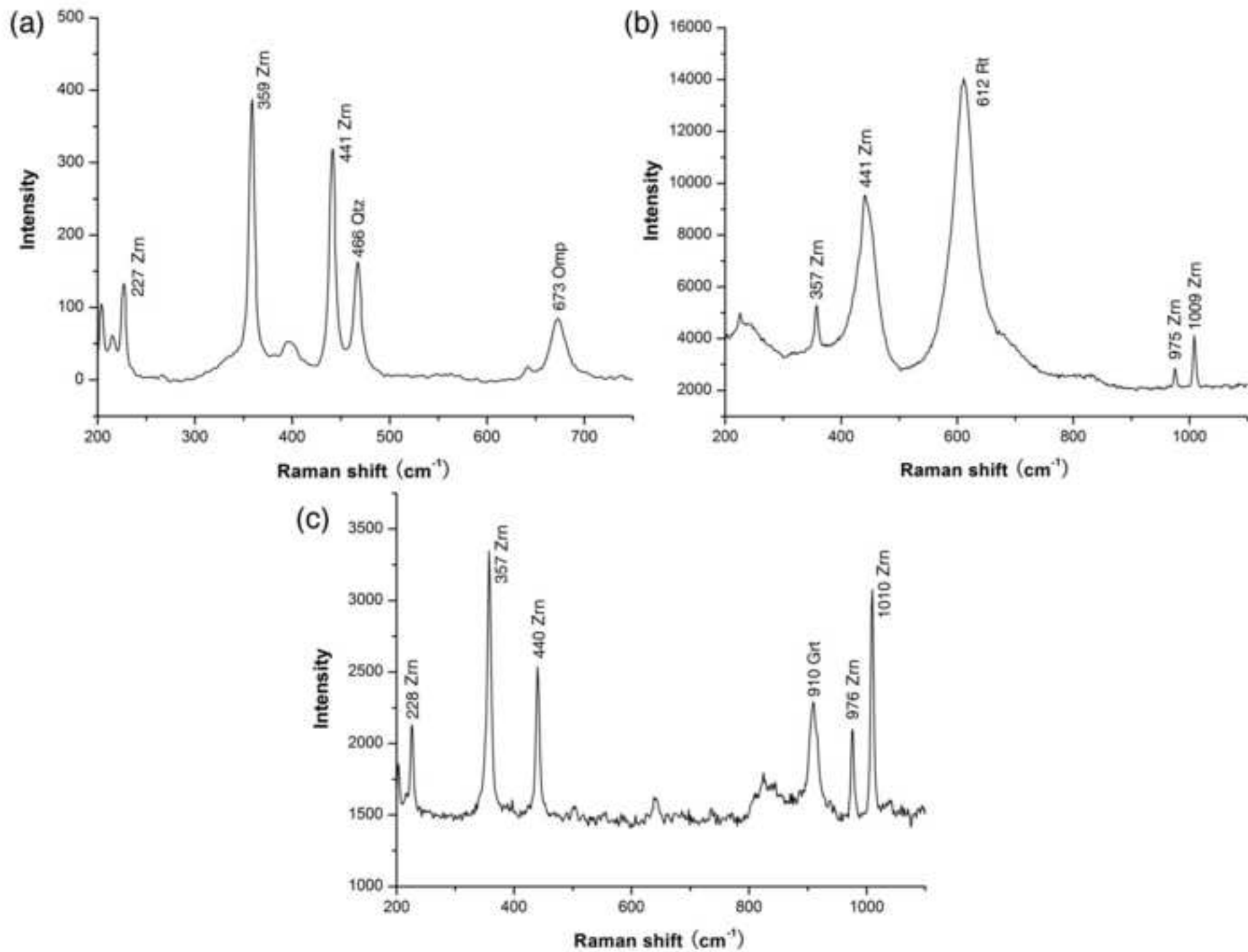


Figure 6
[Click here to download high resolution image](#)

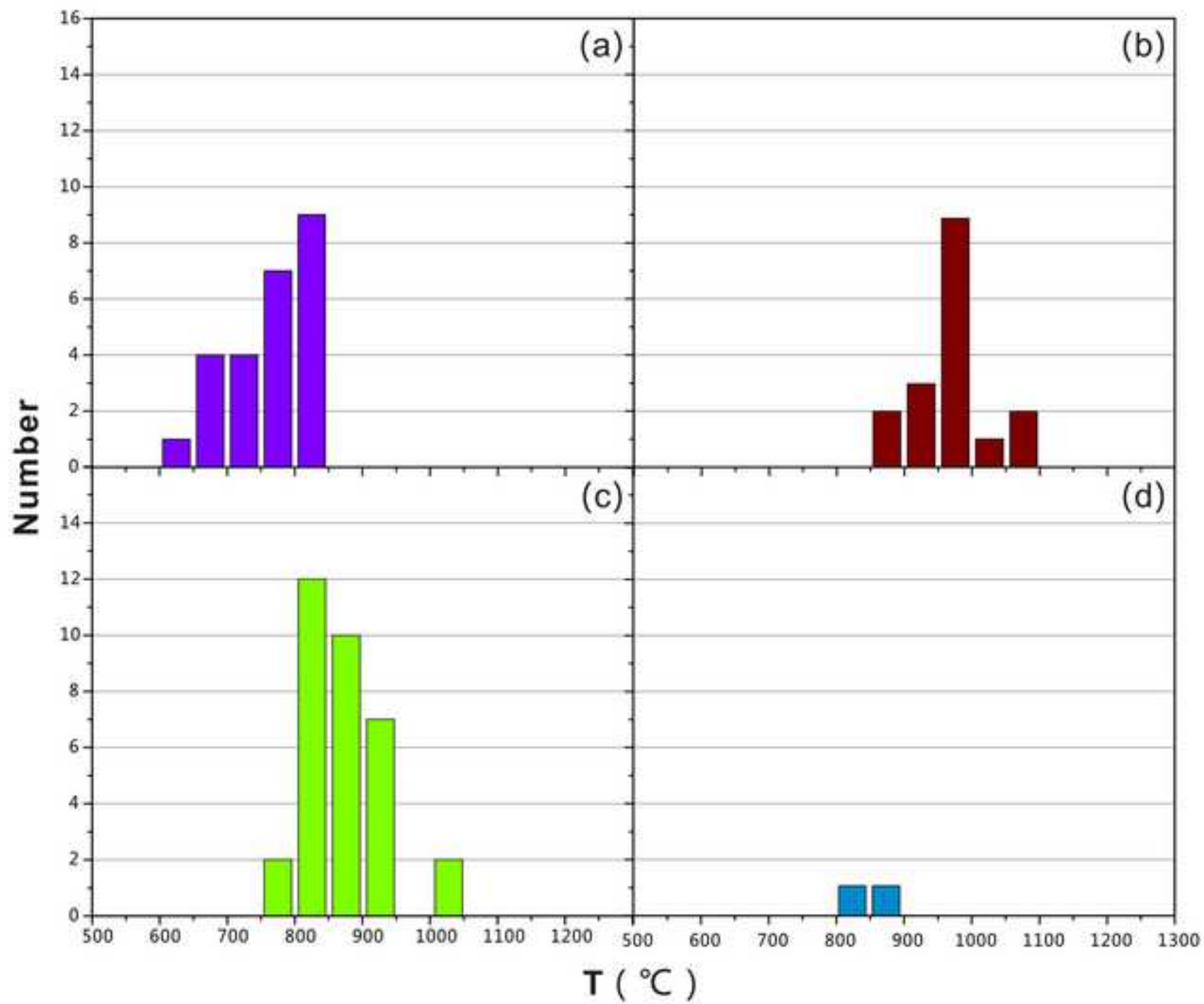


Figure 7
[Click here to download high resolution image](#)

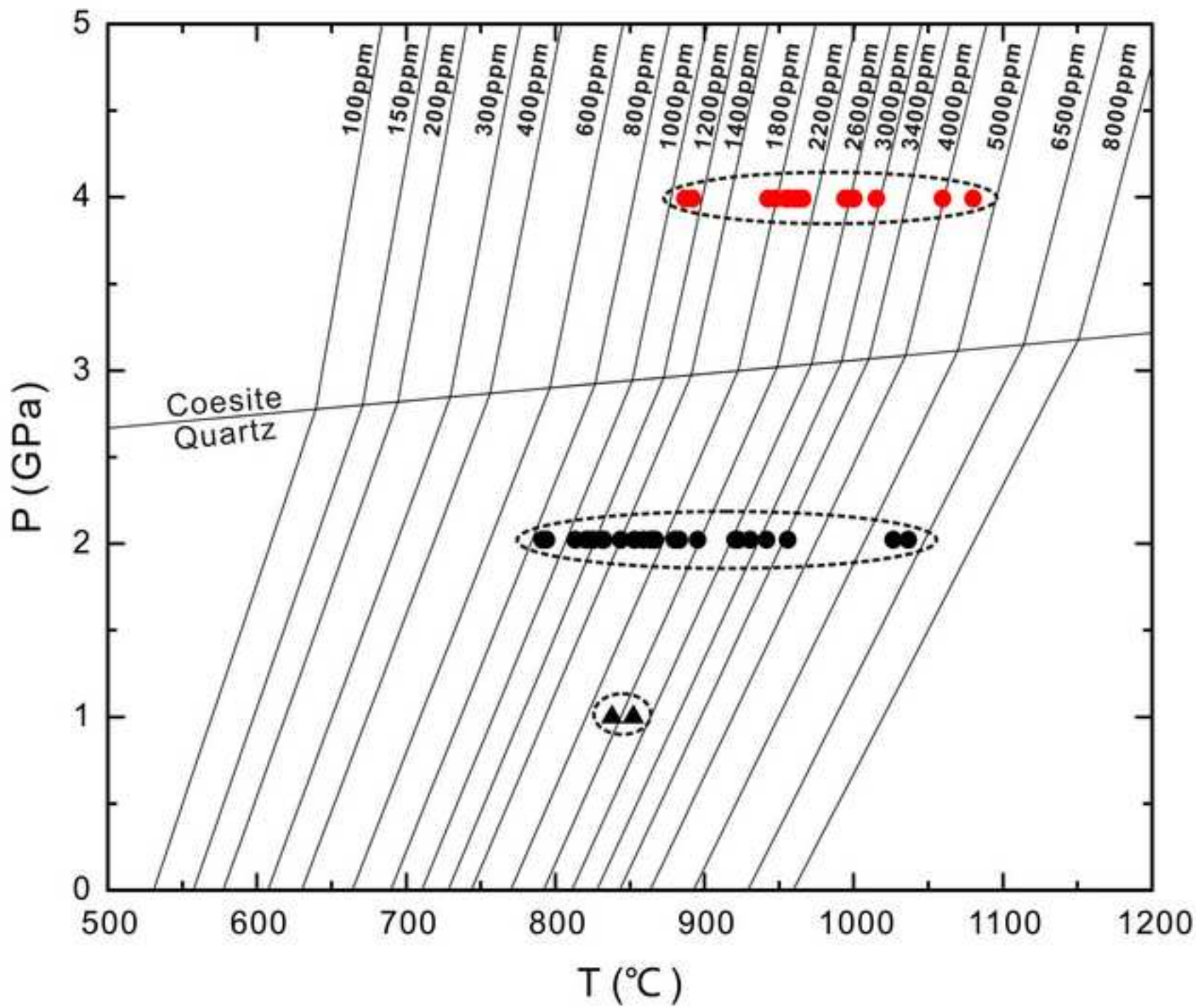


Figure 8
[Click here to download high resolution image](#)

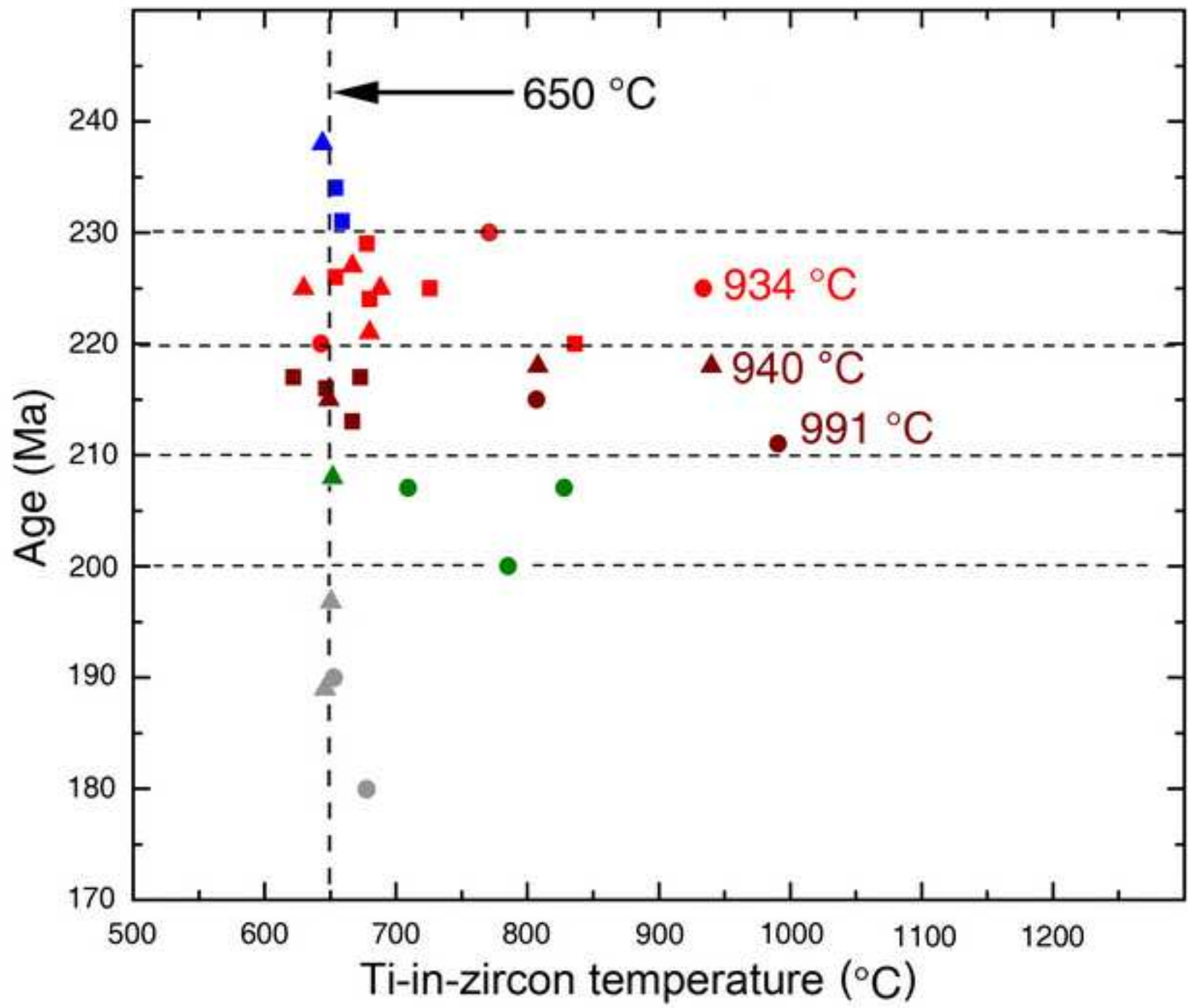


Figure 9
[Click here to download high resolution image](#)

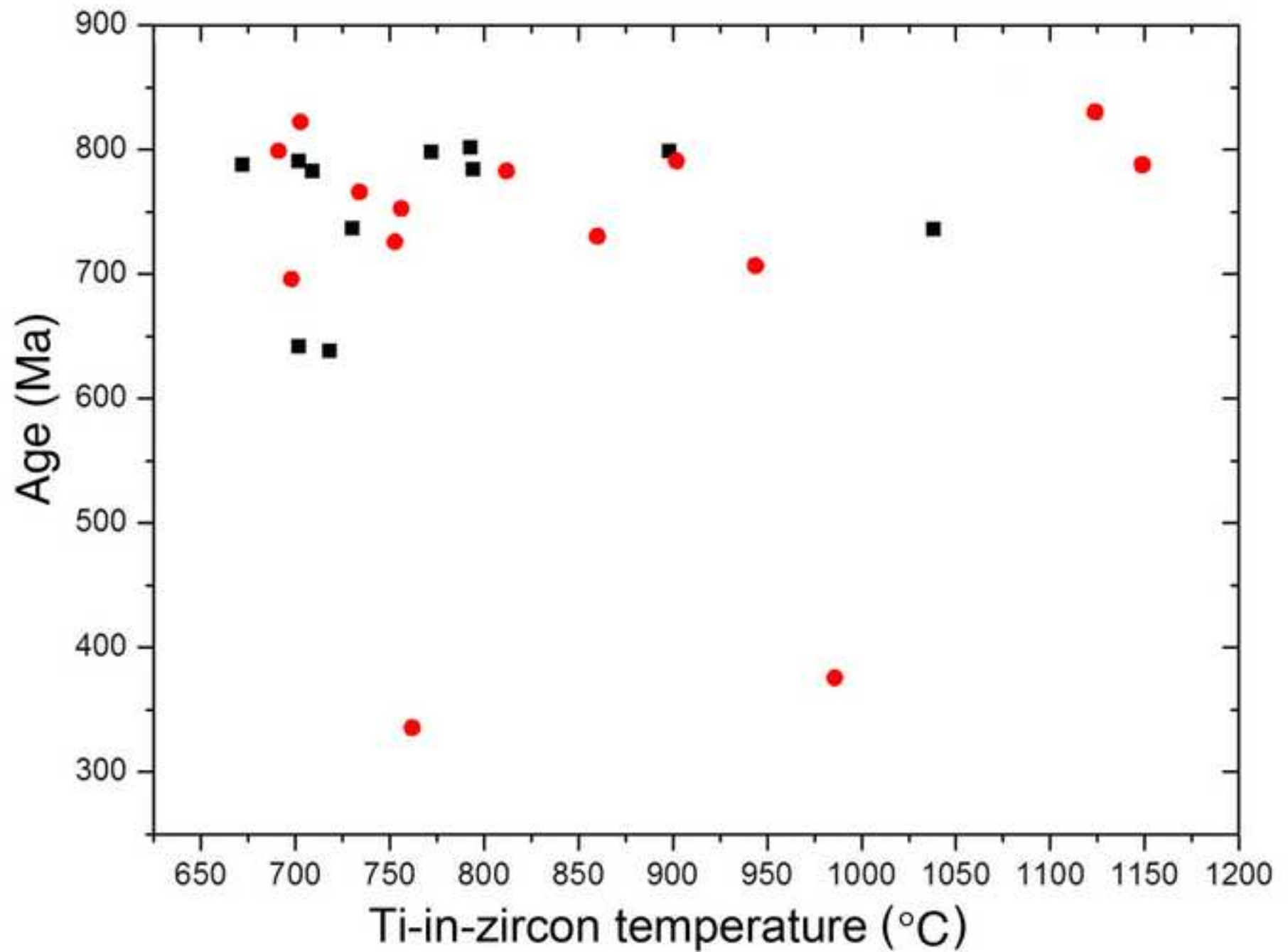


Figure 10
[Click here to download high resolution image](#)

